Spin–State Energetics for Hydride and Helium Models of Transition Metal Complexes: A Benchmark Study of Wave Function Quantum Chemistry Methods

Mariusz Radoń*

Jagiellonian University, Faculty of Chemistry, Gronostajowa 2, 30-387 Kraków, Poland

E-mail: mradon@chemia.uj.edu.pl

Phone: +48 12 6862489

Abstract

Accurate determination of spin–state energetics in first-row transition metal (TM) complexes is recognized as a challenging problem in computational quantum chemistry because different methods often yield divergent predictions and credible reference data are scarce. Trying to provide a way towards unambiguously accurate reference values from high-level wave function computation, a benchmark set of small TM complexes with hydrides (H^-) or helium atoms as σ-donor ligands is presented. These models have analogous electronic structures as realistic TM complexes and their spin–state energetics feature comparable method-dependence, but their small size enables application of more accurate methods than are applicable to realistic TM complexes. The extrapolated full configuration interaction (exFCI) results are obtained for selected spin–state splittings of the hydride/helium models and used as reference values for benchmarking various wave function methods, including second- and third-order perturbation theory multireference methods, multireference CI, and coupled cluster

methods with up to approximate quadruples. It is demonstrated that the exFCI reference values can be reproduced satisfactorily with both multireference and single-reference methods, among which the NEVPT2 and CCSDT(Q)$_\Lambda$ methods perform best, yielding deviations comparable with the uncertainties of the reference values or smaller than 2 kcal/mol. The CCSD(T) method yields errors of ca. 3 kcal/mol or smaller, with one exception where the CCSD(T)'s error is greater than 6 kcal/mol presumably due to pronounced multireference character. The CASPT2, CASPT3, CASPT2/CC methods are shown to not outperform the CCSD(T) method consistently. The present study, in addition to presenting novel benchmark set for the spin–state energetics problem, establishes hydride/helium models of TM complexes as useful and challenging systems for further investigations with correlated electronic structure methods.

1 Introduction

The spin state of a transition metal (TM) complex may profoundly affect its physicochemical properties and is subject to change during chemical reactions, making it of uttermost importance in computational studies to accurately describe the relative energies of alternative spin states.[1–6] Meanwhile, accurate computation of *spin–state energetics* (also termed *spin–state splittings*) is recognized as a challenging problem, particularly for first-row TM complexes: different quantum chemistry methods, including density functional theory (DFT) and wave function theory (WFT) ones, tend to produce divergent results and hence obtaining unquestionable reference data is difficult.[6–12] The problem has been recently tackled by several research groups, including us, who aimed to derive benchmark-quality reference data of spin–state energetics either from high-level theoretical calculations[13–20] or from suitable experimental data.[21–26] The relative merits of the theory-based and experiment-based benchmarks have been reviewed by the present author.[12]

In general, theory-based benchmarks have multiple advantages, including conceptual simplicity, straightforwardness of making comparisons, and easiness of generating computed data for any desired molecular structure.[27] However, a significant limitation in this approach for the problem of TM spin–state energetics is the difficulty of choosing a computational method which is always

sufficiently accurate to provide the reference data, i.e., yields computed energy difference close enough to the full configuration interaction (FCI) limit, and is simultaneously applicable to TM complexes of interest in inorganic/bioinorganic chemistry and materials science.[12] The high-level methods applicable in practical cases are usually limited to single-reference CCSD(T) (coupled cluster with singles and doubles, and noniterative triples),[28] CASPT2 or NEVPT2 (multireference second order perturbation theories based on the complete active space wave function)[29,30] or MRCI+Q (multireference configuration interaction with singles and doubles, including approximate size-consistency correction).[31] Compound methods derived from these approaches, such as CASPT2/CC,[14] CASPT2.5[16] and CASPT2+δMRCI,[20] as well as various quantum Monte Carlo methods[15,32,33] were also advocated for TM complexes. Unfortunately, different "high-level" methods oftentimes lead to divergent predictions of spin–state energetics[12] and, for such large molecular systems as realistic TM complexes, it is usually impossible to certainly determine the true accuracy of the method which is supposedly the most accurate one.[16]

Calculations using higher-level methods can be enabled by reducing the system size, i.e., the number of correlated electrons. Along this line, the group of Truhlar studied gaseous TM ions as simple model systems for the problem of spin–state energetics.[16] However, these atomic systems are very different from molecular TM complexes in terms of the correlation effects that determine their spin–state splittings and hence any conclusions obtained from such atomic benchmarks do not necessarily apply to molecules.[12] Likewise, several studies were focused on the properties of diatomic molecules containing TMs,[34–36] but also diatomics differ considerably from coordinatively-saturated TM complexes, with regard to their electronic structure and relevant correlation effects.

Trying to find a better representation of realistic TM complexes, the present study develops the idea of models in which the ligands are simplistically represented as hydrides (H^-) or helium atoms (He), as these entities may be viewed as the simplest possible donors of the electronic pairs to the metal. The first use of such models in the context of modern WFT methods comes from the study of Feldt et al.,[37] where the $[FeOHe_5]^{2+}$ model was proposed for the sake of comparing coupled cluster (CC) results at the CCSD(T) level with the higher CCSDT(Q) level for the quintet–

triplet energy difference. In this model, He atoms were regarded as simplified models of ammonia ligands present in a more realistic model, $[FeO(NH_3)_5]^{2+}$, of iron-oxo species being involved in the process of C−H bond activation.[37] The similarity of the $[FeOHe_5]^{2+}$ model to $[FeO(NH_3)_5]^{2+}$ was judged from comparison of their spin densities. The same $[FeOHe_5]^{2+}$ model was subsequently used by Benedek et al.[38] in their study of CC methods with different choices of reference orbitals. Most recently, Reimann and Kaupp[20] introduced two other related models with helium ligands, $[FeHe_6]^{2+}$ and $[FeHe_6]^{3+}$ for testing the accuracy of their composite CASPT2+δMRCI method with respect to the MRCI+Q reference.

The present work builds on these ideas to develop a more general benchmark set of octahedral $[MH_6]^{(6-n)-}$ and $[MHe_6]^{n+}$ as well as square-planar $[MH_4]^{(4-n)-}$ complexes as simplified models for the spin–state energetics problem. The hydrides (H^-) or He atoms in these models serve as the simplest possible σ-donor ligands and M^{n+} is a first-row TM ion being the acceptor of these pairs. Despite the simplicity and a small number of correlated electrons (26e for the octahedral case), these models feature analogous electronic structure as real TM complexes with regard to their orbital occupancies in different spin states and the presence of the metal–ligand covalent bonding. It will be also demonstrated that their spin–state energetics have comparable dependence on the choice of method as for realistic TM complexes, making these models valuable targets for extensive benchmarking of WFT methods. After obtaining the complete basis set limits of the spin–state energetics using CASPT2, MRCI+Q and CCSD(T) methods, a smaller basis set will be proposed for further benchmarking of selected energy differences in Fe^{II} complexes. The comparison will include, in addition to CASPT2, NEVPT2, MRCI+Q and CCSD(T), also computationally more expensive methods WFT methods: CCSDT and CCSDT(Q) (i.e., CC with full triples and possibly also noniterative quadruples) as well as ACPF[39] and AQCC[40] (which are size-consistent modifications of the MRCI). The reference values will be estimated FCI energies obtained from selected CI (SCI) approach with the Configuration Interaction using a Perturbative Selection made Iteratively (CIPSI) algorithm.[41–43] Note that CIPSI as well as other related SCI approaches[44–47] are promising methods to obtain a near-FCI energies for small to medium-size molecules.[43,48,49]

The applications of CIPSI described in the literature also include TM-containing molecules and simple TM complexes,[50–53] although this study is probably the first one in which the compelling problem of spin–state energetics is directly addressed using this approach.

It must be stressed that molecules investigated in this work do not attempt to model any particular compound studied by experiment. Complex TM hydrides, such as $[FeH_6]^{4-}$, do exist in solid state compounds, for example $Mg_2[FeH_6]$, and they even have been considered as hydrogen carriers,[54] but the present study is clearly not meant to address the properties of these compounds. The presently studied systems are meant to be minimal models for studying general aspects of the correlation effects relevant to the TM spin–state energetics problem, and thus they have similar status to other artificial models used in quantum chemistry, for instance hydrogen chains or networks, which helped to understand some basic features of electron correlation in the context of DFT.[55]

2 Methods and Models

2.1 Construction of Models

The $[MH_6]^{m-}$ and $[MHe_6]^{n+}$ models used in this work were obtained by placing the appropriate ligands (H^- or He) in the octahedral arrangement around the central first-row TM ion (M), with the metal–ligand distance set to $d = 2$ Å. The same metal–ligand distance was used for the $[FeH_4]^{4-}$ model possessing square-planar geometry. In order to stabilize the electronic structure of the $[MH_6]^{m-}$ complexes, 8 point charges of $+0.5$e were added at the corners of the M-centred cube, each at the distance of $\sqrt{3} \times 1.8 \approx 3.118$ Å from the central ion, maintaining the octahedral symmetry. For $[FeH_4]^{2-}$, analogously 4 point charges $+0.5$e were added at the corners of the M-centered square, each at the distance of 3.1 Å from the central ion, maintaining the D_{4h} symmetry. Sample input files to illustrate the definitions of the models and point-charges are given in Supporting Information. Note that the presently chosen metal–ligand and metal–charge distances are arbitrary and the studied geometries are non-equilibrium ones. Also, for simplicity, all the spin states are computed for the same geometry of the model. These simplifications are made be-

cause our purpose is not to model any particular TM complex, but rather to mimic some general features of TM complexes with octahedral or square-planar geometries. In particular, the present Fe−H/He distance is close to metal-ligand distances found in realistic first-row TM complexes with typical ligands, like amines, and therefore much longer than equilirbrium TM-hydride distance in $Mg_2[Fe^{II}H_6]$ (1.56 Å[54]). The shorter distance leads to greater stabilization of the singlet state, whereas for the present non-equilibrium distance, the singlet and quintet states will be closer in energy.

2.2 Computational Details

All CCSD(T), MRCI+Q, ACPF and AQCC calculations were performed using Molpro,[56] interfaced to MRCC[57] for CCSDT(Q) calculations, whereas CASPT2 calculations were performed using OpenMolcas.[58] The CCSD(T) calculations for open-shell systems correspond to the UCCSD(T) formulation based on the ROHF reference, as implemented in Molpro.[59] In the calculations marked as PBE-CCSD(T), Kohn–Sham orbitals for the PBE functional[60] were used in the reference determinant instead of the default choice of Hartree–Fock (HF) orbitals. In the PBE-CCSD(T) calculations, the open-shell program was used even for singlets to obtain correct (T) energies.

The choice active space used in all multiconfigurational calculations was based on Pierloot's rules for mononuclear TM complexes,[29,61,62] meaning that valence 3d orbitals were active together the double-shell 4d orbitals and two σ-bonding ligand orbitals (or one such orbital in the case of square-planar complex, $[Fe^{II}H_4]^{2-}$) . This leads to the active space (10e,12o) for Fe^{II} and Co^{III} octahedral complexes, (8e,11o) for the square-planar $[FeH_4]^{2-}$ and (9e,12o) for Fe^{III} complexes. The notation (*N*e, *K*o) means that *N* active electrons are distributed in *K* orbitals.

The MRCI+Q calculations (with single and double excitations beyond the active space) were performed using the new internally-contracted formation[63] which is based on the Celani–Werner scheme[64] and is computationally much more efficient than the old MRCI algorithm[65] also available in Molpro. However, the ACPF and AQCC calculations can only be performed within in the old algorithm, making them substantially more expensive, and were carried out accordingly only

for $[Fe^{II}H_6]^{4-}$. In order to reduce the computational cost of these calculations, the 4d orbitals corresponding to empty 3d orbitals (in the leading configuration) were eliminated, leading to the active space (10e,10o) for the singlet, (10e,11o) for the triplet, and unchanged (10e,12o) for the quintet. (This reduction of active space in lower-spin states has only small impact on their energy and similar procedures are commonly used in productive multireference calculations for larger TM complexes, and are often necessary to avoid uncontrolled orbital rotations.) The MRCI+Q calculations employed the Davidson–Silver–Siegbahn (DSS) size-consistency correction, which outperforms the standard Davidson correction in larger TM complexes.[24]

Valence electrons and TM outer-core (3s3p) electrons were correlated, whereas the TM inner-core (1s2s2p) electrons were frozen. All calculations were performed with the non-relativistic Hamiltonian. Although scalar-relativistic effects for spin–state energetics are generally important, they are highly transferable between different theory levels,[19,66,67] therefore not expected to influence the comparisons performed in this study.

Energy extrapolation to the complete basis set (CBS) limit was performed using standard extrapolation formula of Helgaker et al. for the correlation energy[68]

$$E_n = E_{\mathrm{CBS}} + An^{-3}, \tag{1}$$

based on the results obtained with aug-cc-pwCVQZ/aug-cc-pVQZ ($n = 4$) and aug-cc-pwCV5Z/aug-cc-pV5Z ($n = 5$) basis set (where the slash symbol used in the notation of basis sets separates the basis used for TM and ligand atoms). The reference energy was taken from the larger basis set. Other choices of extrapolation formulae were also tested and shown to almost identical extrapolated energy differences at CCSD(T), PBE-CCSD(T) and CASPT2 theory levels (Supporting Information, Tables S2–S4).

The CIPSI calculations were performed using Quantum Package (QP2),[43] to which the second-quantized Hamiltonian has been imported from the Molpro (via the FCIDUMP file format,[69] read using ORBKIT[70] and suitably converted for the `import_integrals` plugin of QP2). The

orbitals used in the CIPSI calculations were natural orbitals resulting from prior CASSCF(10e,12o) or CASSCF(8e,11o) calculations.

3 Results and Discussion

3.1 Electronic Structure

The present hydride and helium models are constructed to have similar electronic structure as realistic TM complexes. In order to demonstrate this similarity, Figure 1(a) shows the contour plots of CASSCF natural orbitals with significant metal 3d character for the example of $[FeH_6]^{4-}$.

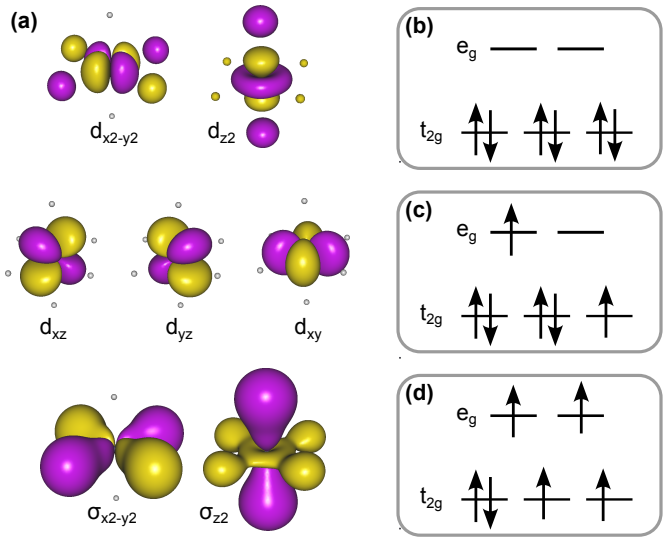

Figure 1: (a) Contour plots of the CAS(10,12) active orbitals for the singlet state of $[Fe^{II}H_6]^{4-}$, omitting the double-shell orbitals; (b–d) schematic orbital occupancies in the leading configuration for the singlet, triplet, and quintet states.

As expected from ligand-field theory, three of the metal 3d orbitals (d_{xz}, d_{yz}, d_{xy}) remain essentially nonbonding, whereas the remaining two ($d_{x^2-y^2}$, d_{z^2}) point centrally towards the ligands and hence become involved in covalent bonding, which leads to formation of bonding and antibonding molecular orbitals (shown in, respectively, the bottom and top part of Figure 1(a)). In square planar model $[FeH_4]^{2-}$, only one of the metal 3d orbitals is involved in the covalent σ-bonding, whereas

the other four remain mostly nonbonding. The mixing between the metal and ligand contributions in the σ-type orbitals, i.e., the degree of bond covalency, is more pronounced for the models with hydride ligands than in those with helium ligands, but is clearly present in both cases. The presence of the discussed σ-bonding is a notable feature of the presently considered models, making them similar to realistic TM complexes[29,62,71] and distinguishing from bare metal ions[16] or ions surrounded only by point charges.[72,73] (By contrast, there is obviously no way to describe π-type orbital interactions, e.g. related to π backdonation, within such models.)

The principal electronic configurations for the three spin states of this octahedral model are schematically shown in panels (b)–(d) of Figure 1. The same configurations apply to all d^6-electron models, i.e., with Fe^{II} and Co^{III} central ions. For the d^5-electron model, i.e., with Fe^{III} central ion, there is one less electron, resulting in the leading configurations $(t_{2g})^5$ for the doublet, $(t_{2g})^4(e_g)^1$ for the quartet, and $(t_{2g})^3(e_g)^2$ for the sextet state. For the square planar complex $[Fe^{II}H_4]^{2-}$, the leading configurations are $(d_{z^2})^2(d_{xz}, d_{yz})^2(d_{x^2-y^2})^2$ for the triplet and $(d_{z^2})^2$ $(d_{xz},d_{yz})^2$ $(d_{x^2-y^2})^1(d_{xy})^1$ for the quintet state (assuming that ligands lie in the $y = \pm x$ directions), analogously to the spin states of four-coordinate Fe^{II} porphyrin.[71]

3.2 Diagnostics of Nondynamic Correlation

Table 1 reports some diagnostics of nondynamic correlation for the studied models in various spin states. The T_1 and D_1 diagnostics[74,75] are two different measures of the singles' contribution to the CCSD wave function, i.e., these diagnostics measure the orbital relaxation effect in response to including the electron correlation, and their large values are often treated as a signal of obtaining potentially less accurate results from single-reference correlation methods.[34,76,77] A related diagnostic is also $|t_{1\,\mathrm{max}}|$, the largest absolute value of the single excitation amplitude at the CCSD level. Analogously, $|t_{2\,\mathrm{max}}|$ is the largest absolute value of the double-excitation amplitude at the CCSD level. The next diagnostic, %MC, directly measures the percentage multiconfigurational character and is defined as $(1 - C_0^2) \times 100\%$, where C_0 is the coefficient of the principal configuration in the CASSCF wave function. Note that in the literature, it is usually defined based on full-valence

Table 1: Diagnostics of Nondynamic Correlation. [a]

complex	state[b]	T_1	D_1	$\lvert t_{1\,\max}\rvert$	$\lvert t_{2\,\max}\rvert$	%MC	M
$[FeHe_6]^{2+}$	1	0.009	0.022	0.021	0.063	10.1	0.084
	3	0.008	0.021	0.026	0.068	12.6	0.170
	5	0.007	0.017	0.025	0.026	1.3	0.018
$[FeH_6]^{4-}$	1	0.087	0.234	0.189	0.041	12.1	0.071
	3	0.069	0.250	0.204	0.051	12.1	0.108
	5	0.041	0.121	0.171	0.040	2.5	0.026
$[FeHe_6]^{3+}$	2	0.020	0.071	0.079	0.080	29.1	0.365
	4	0.018	0.072	0.103	0.059	10.3	0.176
	6	0.011	0.032	0.045	0.030	0.6	0.006
$[FeH_6]^{3-}$	2	0.085	0.259	0.276	0.069	21.4	0.186
	4	0.073	0.284	0.413	0.085	20.4	0.266
	6	0.066	0.224	0.317	0.080	4.0	0.044
$[CoH_6]^{3-}$	1	0.096	0.295	0.200	0.060	17.2	0.145
	3	0.080	0.291	0.417	0.112	25.5	0.340
	5	0.053	0.246	0.347	0.099	9.8	0.118
$[FeH_4]^{2-}$	3	0.065	0.272	0.287	0.051	10.1	0.101
	5	0.034	0.137	0.194	0.027	2.0	0.025

[a]Calculated at the CCSD level (T_1, D_1, $|t_{1\,\max}|$, $|t_{2\,\max}|$) or CASSCF level (%MC, M) using the aug-cc-pwCQZ/aug-cc-pVQZ basis set for metal/ligand atoms. [b]Spin multiplicity $2S+1$.

active space,[78] making it impractical in larger molecules, whereas here the %MC diagnostic is calculated based on the standard active space of 12 orbitals, analogously as in the previous study of realistic TM complexes.[24] Finally, the M diagnostic[79] is based on occupation numbers of the CASSCF natural orbitals and measures their deviations from the ideal values at the HF level: 2 for the highest doubly-occupied orbital, 0 for the lowest unoccupied one, and 1 for singly-occupied ones. Although these and related diagnostics do *not* quantitatively correlate with the accuracy obtained in single-reference calculations, e.g., at the CCSD(T) level,[12,36,78,80] they are frequently used in the literature to assess the importance of nondynamic correlation, which is often associated with a multireference character. For the review of the diagnostics and their interpretations, the reader is referred to refs 34,78,81 and references therein.

The diagnostics reported in Table 1 turn out to be comparable and, in some cases, even larger in magnitude than those observed for realistic TM complexes.[24,72,77,78,82] As an illustration, for TM complexes studied in ref 24, the T_1 diagnostics were in range 0.02–0.03; the D_1 diagnostics were in range 0.06–0.17; the M diagnostics were in range 0.01–0.07; and the %MC diagnostics were in range 0.8–8.1 %. Moreover, as in realistic TM complexes, the larger values of diagnostics are typically observed in the low- or intermediate-spin than in the high-spin states (although it is not true in general than a lower-multiplicity state has always a greater value of the diagnostic than a higher-multiplicity state; counterexamples can be easily located in Table 1). Considering the diagnostics based on single-excitation amplitudes (T_1, D_1, $|t_{1\,\mathrm{max}}|$), the larger values are observed for hydride models, which is due to a greater covalency of their metal-ligand bonds (see Section 3.1). Whereas for helium models, the T_1 is always below 0.02 and D_1 is below 0.08, the largest T_1 values observed for hydride models are close to 0.1, and the largest D_1 values are nearly 0.3. The latter values are far above than commonly used criteria $T_1 < 0.05$ and $D_1 < 0.15$, which were suggested in the literature for reliable single-reference calculations.[78] The %MC and M diagnostics based on the CASSCF wave function are largests for the models with +3 metal ions: in their low- and intermediate-spin states, the leading configuration accounts for only 70–85 % of the CASSCF wave function. This is in contrast to the high-spin state, which is to better than 90 % singly-

configurational in all cases. Note that both %MC and M diagnostics take their maximum values for the low-spin state of $[Fe^{III}He_6]^{3+}$, which is characterized by rather small values of the T_1, D_1, and $|t_{1\,max}|$ diagnostics. The corresponding hydride complex, $[Fe^{III}H_6]^{3-}$, is marked by relatively large values of all the diagnostics (in the doublet and quartet states). Overall, the diagnostics obtained here suggest that the presently considered hydride and heliium models may suffer from considerable nondynamic correlation effects.

It has also been proposed to link the importance of nondynamic correlation with the sensitivity of DFT-computed energy differences to the admixture of the exact exchange (EE).[81,83] To illustrate this EE-dependence for presently studied models, Table 2 shows the energy differences computed at the DFT level with the PBE and PBE0 functionals, which contain 0% and 25% of the EE, respectively. The difference between the PBE and PBE0 results is similar to the B_1 diagnostics of Truhlar with co-workers (which is analogous based on the BLYP and B1LYP pair of functionals).[83]

Table 2: DFT Results with PBE and PBE0 Functionals (kcal/mol). [a,b]

	PBE	PBE0	difference[c]
$^{1,3}[FeHe_6]^{2+}$	−23.6	−26.7	3.1
$^{1,5}[FeHe_6]^{2+}$	−69.7	−80.0	10.3
$^{1,3}[FeH_6]^{4-}$	11.6	−2.9	14.5
$^{1,5}[FeH_6]^{4-}$	14.5	−20.4	34.9
$^{2,4}[FeHe_6]^{3+}$	−34.8	−43.4	8.6
$^{2,6}[FeHe_6]^{3+}$	−84.9	−111.1	26.2
$^{2,4}[FeH_6]^{3-}$	10.6	−6.6	17.2
$^{2,6}[FeH_6]^{3-}$	21.0	−9.2	30.2
$^{1,3}[CoH_6]^{3-}$	22.1	3.0	19.0
$^{1,5}[CoH_6]^{3-}$	44.4	11.3	33.1
$^{3,5}[FeH_4]^{2-}$	7.6	−10.2	17.8

[a] Spin-unrestricted calculations, using the aug-cc-pwCVTZ/aug-cc-pVTZ basis set for metal/ligand atoms. [b] All energy differences defined as in eq. (2) below, values in kcal/mol. [c] Defined as $\Delta E(\mathrm{PBE}) - \Delta E(\mathrm{PBE0})$.

As is typically observed in TM complexes,[7,84] the increasing admixture of the EE leads to relative stabilization of the higher-spin states with respect to lower-spin states. The sensitivity

to the EE admixture observed for the present hydride models is quite remarkable: the difference between PBE and PBE0 results, corresponding to the 25%-difference in the EE admixture, is about 30 kcal/mol for the energy differences with $\Delta S = 2$ (quintet–singlet, sextet–doublet) and about 15–20 kcal/mol for the energy differences with $\Delta S = 1$ (triplet–singlet, quintet–triplet, quartet–doublet). This is comparable to the sensitivity observed in the series of 30 Fe SCO complexes studied by Kepp,[21] who found the effect of around 1 kcal/mol per 1% of the admixed EE (for energy differences with $\Delta S = 2$). A somewhat smaller sensitivity is observed for helium models.

We further note that the strong sensitivity of DFT spin–state energetics to the EE admixture is rooted in the correlation effects in the metal–ligand bond[85,86] and this phenomenon is *not* observed[85] for TM ions surrounded by point charges, illustrating the clear advantage of the present hydride/helium models. Moreover, somewhat parallel to the effect of EE admixture, we also observe that the outer-core correlation effects due to 3s3p electrons (Δ3s3p) differ considerably between CCSD(T) and CASPT2 (Table S1, Supporting Information), which is another similarity of the present models to realistic TM complexes.[14,73]

3.3 Spin–State Energetics in the CBS Limit and Their Method-Dependence

Table 3 reports the spin–state energetics of considered models extrapolated to the complete basis set (CBS) limit. These calculations were performed using four typical WFT methods which are also applicable to larger TM complexes:[24,25] CASPT2, MRCI+Q, CCSD(T) and PBE-CCSD(T). The first two methods are multireference approaches based on the CASSCF wave function with the standard choice of active space (see Section 2); CCSD(T) is a well-known "gold standard" approach in quantum chemistry; and the last method is a variant of it based on the PBE reference orbitals instead of the default choice of HF orbitals. All the energy differences are defined as

$$\Delta E = E(\text{higher-spin}) - E(\text{lower-spin}), \tag{2}$$

e.g., the $^{1,3}[Fe^{II}H_6]^{4-}$ energy difference is understood as $E(\text{triplet}) - E(\text{singlet})$.

Table 3: Spin–State Energetics in the CBS Limit. [a,b]

	CASPT2	MRCI+Q(DSS)	CCSD(T)	PBE-CCSD(T)	$\sigma_{\Delta E}$ [c]
$^{1,3}[FeHe_6]^{2+}$	−25.2	−20.1	−20.7	−20.5	2.4
$^{1,5}[FeHe_6]^{2+}$	−80.3	−70.0	−73.4	−73.1	4.3
$^{1,3}[FeH_6]^{4-}$	4.2	6.7	10.0	17.2	5.7
$^{1,5}[FeH_6]^{4-}$	−10.7	−6.3	−1.7	10.2	9.0
$^{2,4}[FeHe_6]^{3+}$	−39.6	−37.5	−41.7	−40.4	1.8
$^{2,6}[FeHe_6]^{3+}$	−126.5	−119.2	−124.7	−122.8	3.1
$^{2,4}[FeH_6]^{3-}$	2.9	3.7	2.4	4.9	1.1
$^{2,6}[FeH_6]^{3-}$	1.6	2.8	3.5	5.3	1.5
$^{1,3}[CoH_6]^{3-}$	16.8	17.9	19.5	23.2	2.8
$^{1,5}[CoH_6]^{3-}$	30.6	32.1	36.7	39.3	4.0
$^{3,5}[FeH_4]^{2-}$	−10.3	−8.3	−7.9	−5.8	1.8

[a]Values in kcal/mol. [b]See Section 2 for details of the CBS extrapolation. [c]Standard deviation in the sample of ΔE values obtained with the four methods (see text).

It is evident from Table 3 that spin–state energetics for the present set of models are quite diverse. For helium models, the higher spin states are significantly more stable than the lower spin states, resulting in the ΔE values being strongly negative. For hydride models, the ΔE values are closer to zero, sometimes positive, indicating a more considerable stabilization of the lower-spin states. This is rooted a greater t_{2g}–e_g splitting of the metal 3d orbitals exerted by their negatively-charged H^- ligands and also related to a stronger covalency of the metal–ligand bonds in hydride models (see Section 3.1). Moreover, in agreement with the spectrochemical series of metals, the singlet state of $[Co^{III}H_6]^{3-}$ is considerably more stable than in the case of isoelectronic $[Fe^{II}H_6]^{3-}$. The low-spin state is more strongly stabilized with respect to the high-spin state in the case of $[Fe^{III}H_6]^{3-}$ than for $[Fe^{II}H_6]^{4-}$ in agreement with a greater bond covalency in the former case, but note that a similar trend is not observed for the corresponding pair of helium models.

As the present models are artificial molecules, we do not bring much significance to the numeric ΔE values, but rather to their method-dependence: it is clearly seen from the data in Table 3 that different methods lead to divergent results with discrepancies up to several kcal/mol, which mimics the well-known behavior of real TM complexes.[12] This method-dependence can be objectively measured using the standard deviation calculated from the sample of ΔE values computed using the

four methods considered. The resulting standard deviations ($\sigma_{\Delta E}$) are reported in the last column of Table 3. The greatest method-dependence is observed for the $^{1,5}[FeH_6]^{4-}$ energy difference. A smaller, yet still pronounced method-dependence is observed for the $^{1,3}[FeH_6]^{4-}$, $^{1,5}[FeHe_6]^{2+}$, and $^{1,5}[CoH_6]^{3-}$ energy differences. By contrast, very small method dependence is observed for both energy differences of $[Fe^{III}H_6]^{3-}$. For example, the CASPT2 and CCSD(T) results agree to within 1 kcal/mol although for other cases they generally differ by at least a few kcal/mol. This behavior is somewhat surprising as the $[Fe^{III}H_6]^{3-}$ model features a very significant multireference character according to all common diagnostics (see Table 1 in Section 3.2) and thus one might expect that single-reference CCSD(T) calculations should yield significantly different results from multireference methods, but this is not the case.

3.4 Small Basis Set for Comparative Calculations

For further comparative calculations, a moderately-sized basis set b has to be chosen in order to satisfy the two conditions: (1) this basis set should be small enough to enable computationally most expensive methods, but on the other hand, (2) it should be still flexible enough to approximately preserve discrepancies between different methods (m and n) observed in the CBS limit, i.e.,

$$\Delta E_{m/\mathrm{CBS}} - \Delta E_{n/\mathrm{CBS}} \approx \Delta E_{m/b} - \Delta E_{n/b}. \tag{3}$$

Note that eq. (3) can be reformulated to the BSIE transferability condition,[87]

$$\delta_b^m \approx \delta_b^n, \tag{4}$$

where $\delta_b^m = \Delta E_{m/b} - \Delta E_{m/\mathrm{CBS}}$ is the basis set incompleteness error (BSIE) of the energy difference calculated with method m using basis set b and δ_b^n is defined analogously. The approximation defined in eq. (3) or equivalent eq. (4) is well established in quantum chemistry:[87] it is the cornerstone of various composite approaches,[88–90] in which the most expensive method is only applied using a small basis set; it also simplifies performing benchmark studies due to the fact that FCI or nearly-

FCI-quality calculations (to provide the reference values) are only affordable using relatively small basis sets.[45,48,91]

After some experimentation, it was decided to choose for further calculations a composite basis set labeled aT/D′, which is obtained from aug-cc-pVTZ (with omitted g functions and diffuse f functions) for TM atoms combined with aug-cc-pVDZ (without d functions) for ligands.[92] Sample Molpro input file showing definition of this basis set is provided in Supporting Information. Table 4 gives the BSIE of the energy differences calculated with the four methods discussed above when using the aT/D′ basis set. If the BSIE transferability condition of eq. (4) was exactly satisfied, the BSIE values should be method-independent. To measure deviations from this ideal behavior, the last column contains the standard deviations in the sample of BSIEs obtained using the four methods tested (σ_{BSIE}).

Table 4: BSIEs for Spin–State Energetics Calculated Using aT/D′ Basis Set. [a,b]

	CASPT2	MRCI+Q(DSS)	CCSD(T)	PBE-CCSD(T)	σ_{BSIE} [c]
$^{1,3}[FeHe_6]^{2+}$	−0.8	−1.9	−1.9	−2.0	0.6
$^{1,5}[FeHe_6]^{2+}$	−3.6	−5.1	−4.2	−4.4	0.6
$^{1,3}[FeH_6]^{4-}$	−2.7	−2.9	−3.0	−4.2	0.7
$^{1,5}[FeH_6]^{4-}$	−6.7	−6.4	−6.6	−8.7	1.1
$^{2,4}[FeHe_6]^{3+}$	−2.9	−3.5	−2.4	−2.5	0.5
$^{2,6}[FeHe_6]^{3+}$	−7.6	−8.3	−6.8	−7.0	0.7
$^{2,4}[FeH_6]^{3-}$	−3.4	−3.4	−3.2	−2.9	0.2
$^{2,6}[FeH_6]^{3-}$	−7.4	−6.3	−6.4	−6.2	0.6
$^{1,3}[CoH_6]^{3-}$	−2.9	−2.9	−2.3	−3.3	0.4
$^{1,5}[CoH_6]^{3-}$	−4.6	−4.3	−3.5	−5.6	0.8
$^{3,5}[FeH_4]^{2-}$	−5.4	−4.9	−5.4	−6.7	0.8

[a]Values in kcal/mol. [b]Energy differences calculated using the aT/D' basis set can be found in Table S5, Supporting Information. [c] Standard deviation in the sample of BSIE values obtained with the four methods (see text).

As follows from Table 4, the BSIE values of different methods are similar for a given energy difference, resulting in the σ_{BSIE} values being usually well below 1 kcal/mol. The largest σ_{BSIE} value of 1.1 kcal/mol is obtained for the $^{1,5}[FeH_6]^{4-}$ energy difference, which is also the most sensitive one to the choice of method (cf Table 3, $\sigma_{\Delta E} = 9.0$ kcal/mol). In all cases, the σ_{BSIE} values are smaller (in many cases, by several times) than the previously discussed $\sigma_{\Delta E}$ values,

describing variability of the calculated energy differences with the choice of method. Satisfying this condition (i.e., $\sigma_{\mathrm{BSIE}} < \sigma_{\Delta E}$) warrants the bias introduced by an imperfect transferability of the BSIE between different methods is smaller than intrinsic discrepancies between the energies obtained from these methods in the CBS limit.

It is clear that even lower σ_{BSIE} values could be obtained using a larger basis set, for example aug-cc-pwCVTZ/aug-cc-pVDZ (for TM/ligands, respectively); see Table S6, Supporting Information. Nevertheless, it was decided to use the above aT/D′ basis set in order to reduce the time of the computationally most expensive calculations. The number of contractions of the aT/D′ basis for the six-ligand models is only 122, to be compared with 181 for the aug-cc-pwCVTZ/aug-cc-pVDZ basis set; given that 18–20 of these orbitals are occupied, this difference corresponds to even more considerable reduction in the size of the virtual space when comparing the two basis sets.

Finally, one should note that the BSIE transferability condition, eq. (4) is not trivial to satisfy in smaller basis sets. In particular, this condition is considerably violated when using the popular def2-SVP basis set (which has only 73 contractions for the six-ligand models). Already a glimpse at the results shows that differences between different methods observed in the CBS limits are *not* recovered properly in the def2-SVP basis set (Table S7, Supporting Information). For example, for the $^{1,3}[FeH_6]^{4-}$ energy difference, the MRCI+Q and CCSD(T) results in the def2-SVP basis set agree with each other to within 0.1 kcal/mol, although the results of the two methods diverge by 2.7 kcal/mol in the CBS limit. The same problem can be observed with the CCSD(T) results based on different reference orbitals. Thus, method benchmarking in such a small basis set as def2-SVP will not reflect the performance of methods in the CBS limits for the present hydride/helium models. We note that the usage of comparably small basis sets, for example 6-31G*[52] or even minimal one,[93] is quite common for (nearly-)FCI calculations published in the literature. The present approach, based on comparing the $\sigma_{\Delta E}$ and σ_{BSIE} values calculated using a few representative methods, can be used to conveniently check the validity of the BSIE transferability condition in practical cases.

3.5 CIPSI Calculations to Provide Extrapolated FCI Energies

Having chosen above the small basis set aT/D′ for further benchmarking of methods, we performed CIPSI calculations[41–43] to obtain extrapolated FCI (exFCI) energies. Due to their high computational cost, the CIPSI calculations were only performed for selected energy differences: $^{1,3}[Fe^{II}He_6]^{2+}$, $^{1,5}[Fe^{II}He_6]^{2+}$, $^{1,3}[Fe^{II}H_6]^{4-}$, $^{1,5}[Fe^{II}H_6]^{4-}$, $^{1,5}[Co^{III}H_6]^{3-}$, $^{2,6}[Fe^{III}H_6]^{3-}$, and $^{3,5}[Fe^{II}H_4]^{2-}$. This set includes energy differences which are most variable with the choice of method (in terms of the $\sigma_{\Delta E}$ values discussed above). The singlet–quintet splitting in the chosen octahedral models are also most interesting in the context of Fe^{II} spin-crossover complexes,[19,24,66] whereas the triplet–quintet splitting for $^{3,5}[Fe^{II}H_4]^{2-}$ is relevant for ground-state determination in square-planar Fe^{II} porphyrins.[72,87,94] The doublet–sextet splitting for $[Fe^{III}H_6]^{3-}$ is also included as an example of Fe^{III} system with very considerable multireference character in the doublet state, according to the %MC and M diagnostics discussed in Section 3.2.

The CIPSI algorithm (see ref 43 for overview) approaches the FCI energy by an iterative procedure combining variational configuration interaction (CI) with Epstein–Nesbet second-order perturbation theory (PT2). In each iteration, a CI calculation is performed within a subspace of the Hilbert space and the resulting zero-order energy ($E^{(0)}$) is corrected using the PT2 estimate of the residual correlation energy ($E^{(2)}$). to provide the estimate of the total energy. Subsequently, the set of Slater determinants which contribute most significantly to the PT2 energy is added to the variational CI space for the next iteration. This procedure is continued until $|E^{(2)}|$ drops below the threshold or the maximum number of determinants allowed in the CI space is reached. As the second-order energy vanishes in the limit of complete variational space (i.e., the FCI limit), it was proposed to estimate the FCI energy by performing extrapolation of the CIPSI energy as a function of the second-order energy to the zero-limit.[43,48,95] The use of renormalized second-order energy (rPT2, $ZE^{(2)}$) was proposed to improve the extrapolation,[43] as it leads to more balanced estimate of the residual correlation energy for smaller CI wave functions.

The CIPSI results for the investigated electronic states of $[FeHe_6]^{2+}$, $[FeH_6]^{4-}$, $[CoH_6]^{3-}$, $[FeH_4]^{2-}$ and $[FeHe_6]^{3+}$ are shown in Figures 2–6. (Total energies are provided in Tables S10–S19,

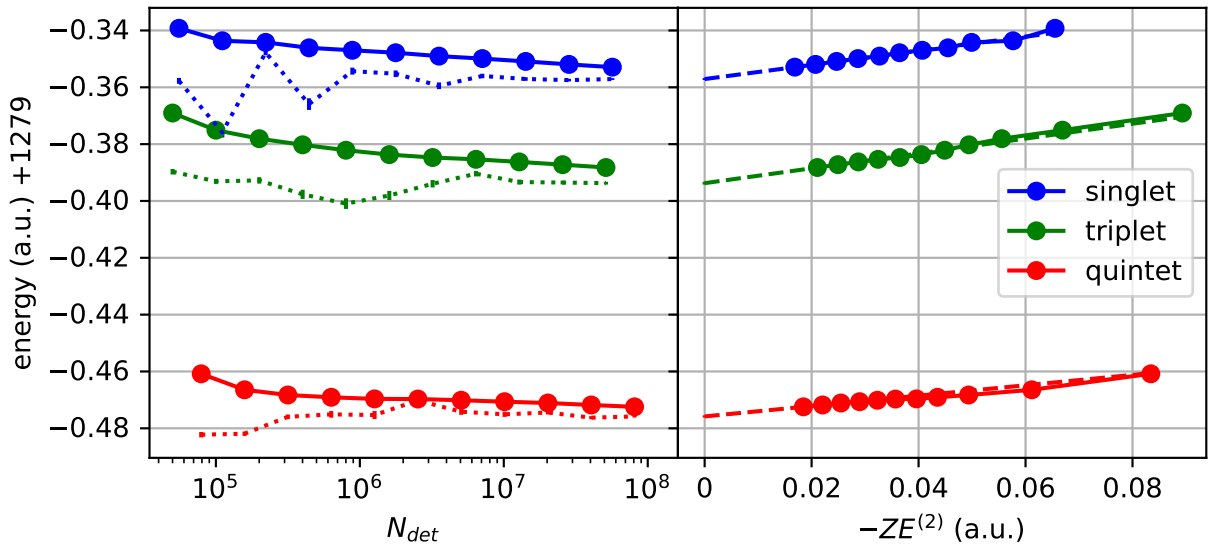

Figure 2: Convergence of CIPSI total energies for the singlet, triplet and quintet states of $[FeHe_6]^{2+}$ with respect to dimension of the variational CI space (N_{det}; *left*) and with respect to the rPT2 energy ($-ZE^{(2)}$; *right*). The latter dependence is used to provide exFCI energies by linear extrapolation to the $ZE^{(2)} = 0$ limit based on two largest available CI wave functions. Dotted lines in the left part show dependence of such extrapolated energies on the maximum value of N_{det} used in the extrapolation.

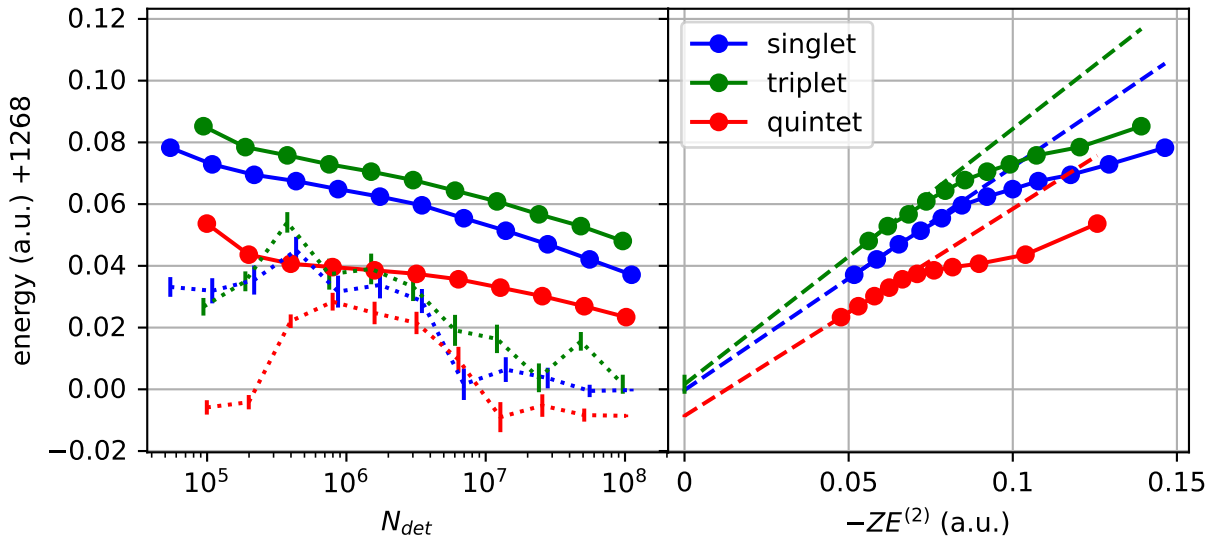

Figure 3: Convergence of CIPSI total energies for the singlet, triplet and quintet states of $[FeH_6]^{4-}$ with respect to dimension of the variational CI space (N_{det}; *left*) and with respect to the rPT2 energy ($-ZE^{(2)}$; *right*). See caption of Figure 2 for additional explanations.

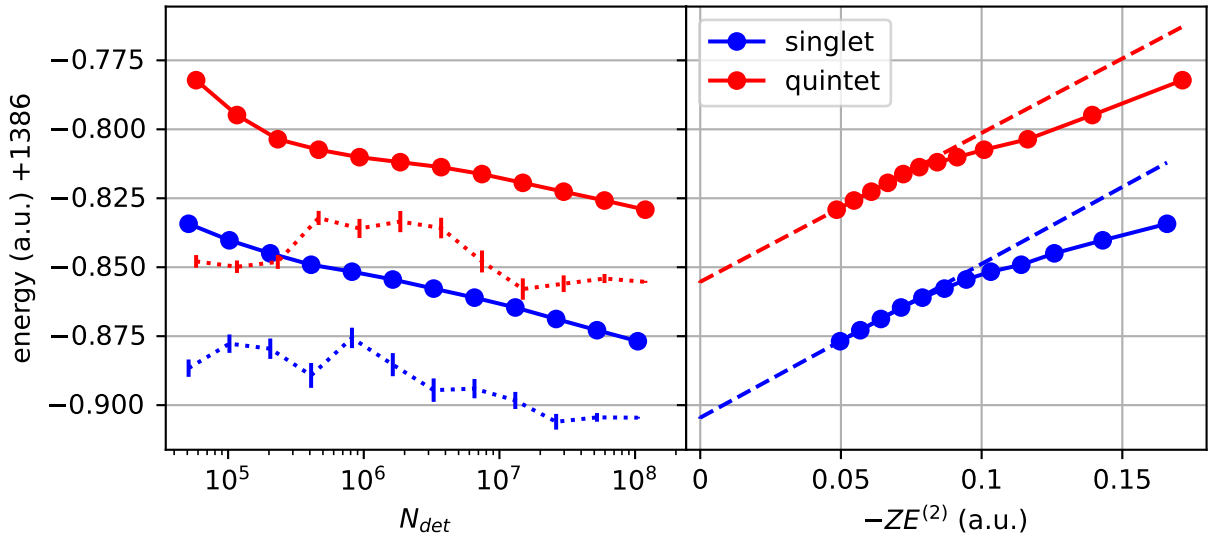

Figure 4: Convergence of CIPSI total energies for the singlet and quintet states of $[CoH_6]^{3-}$ with respect to dimension of the variational CI space (N_{det}; *left*) and with respect to the rPT2 energy ($-ZE^{(2)}$; *right*). See caption of Figure 2 for additional explanations.

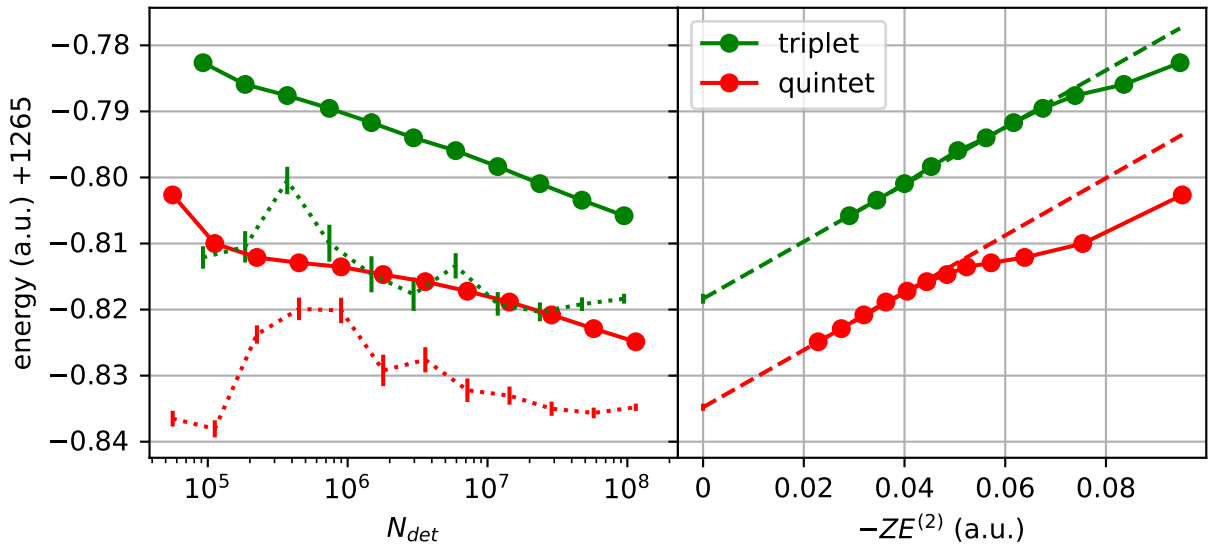

Figure 5: Convergence of CIPSI total energies for the triplet and quintet states of $[FeH_4]^{2-}$ with respect to dimension of the variational CI space (N_{det}; *left*) and with respect to the rPT2 energy ($-ZE^{(2)}$; *right*). See caption of Figure 2 for additional explanations.

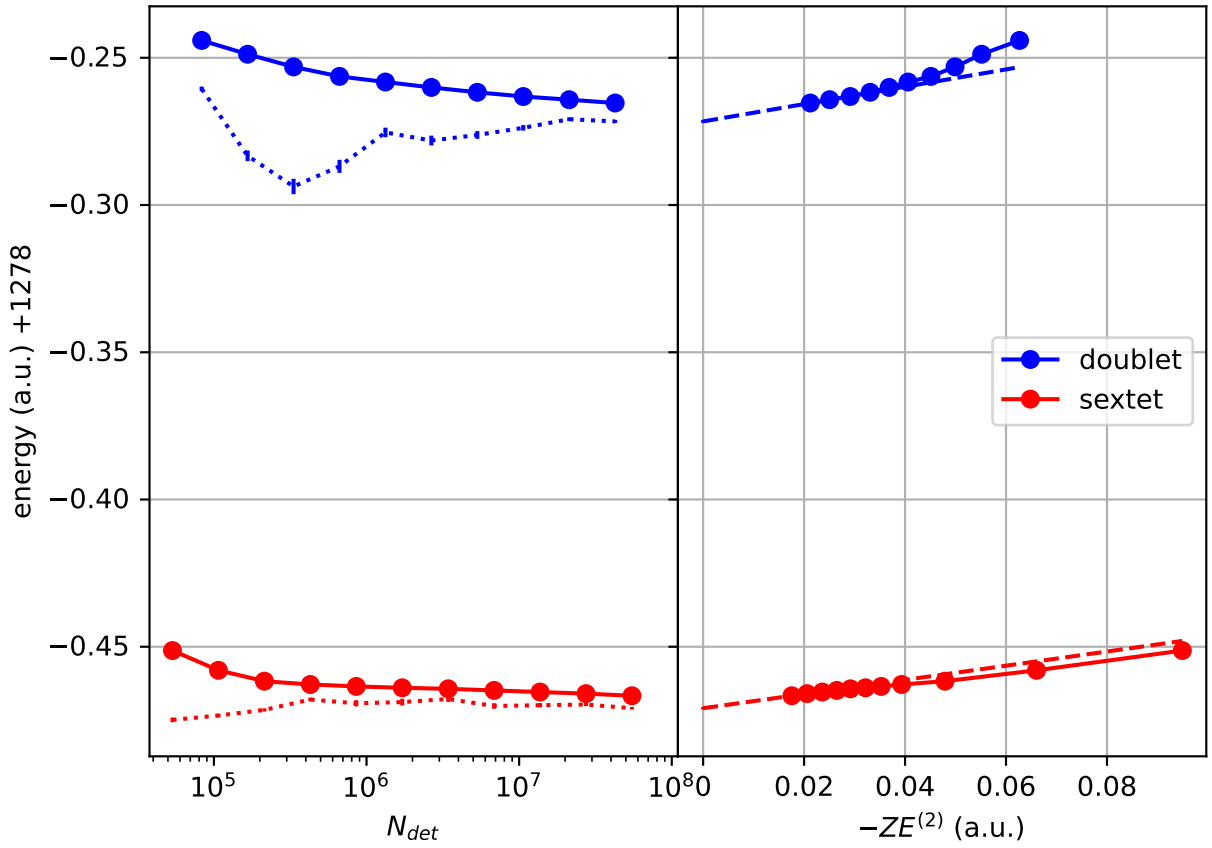

Figure 6: Convergence of CIPSI total energies for the doublet and sextet states of $[FeHe_6]^{3+}$ with respect to dimension of the variational CI space (N_{det}; *left*) and with respect to the rPT2 energy ($-ZE^{(2)}$; *right*). See caption of Figure 2 for additional explanations.

Supporting Information.) In each figure, the left part shows how the CIPSI total energy ($E^{\mathrm{CIPSI}} = E^{(0)} + ZE^{(2)}$) of each state depends on the dimension of the CI space (N_{det}), whereas the right part shows how it depends on the negative of the rPT2 estimate of the residual correlation energy ($-ZE^{(2)}$). A linear extrapolation of the latter dependency using two largest CI wave functions, i.e., two points with the smallest $-ZE^{(2)}$ values, is shown as a dashed line and is used to provide the exFCI total energy of each state. The dotted curves (to the left) show how such extrapolated energies depend on the dimension of the CI space.

It is clear from Figure 2 that $[FeHe_6]^{2+}$ is an example of a well behaving system: the CIPSI estimates of total energies approach constant values to within 0.01 a.u. and, even if they are not fully converged, the residual correlation energies drop below 0.02 a.u. with the CI wave function of about 5×10^7 Slater determinants. Moreover, the CIPSI energies are nearly linear functions of the residual correlation energy and the extrapolation lines for different states are nearly parallel. By contrast, the case of $[FeH_6]^{4-}$ (Figure 3) is considerably more challenging: the CIPSI total energies are far from convergence even with 10^8 determinants; the second-order energy correction to be overcome by the extrapolation procedure is still 0.05 a.u. and the extrapolation lines for different states are considerably non-parallel, resulting in less accurate extrapolated energy differences. The case of $[CoH_6]^{3-}$ (Figure 4) seems to be comparably challenging as $[FeH_6]^{4-}$ and the case of $[FeH_4]^{2-}$ (Figure 5) is somewhere in between these two.

Table 5 shows the exFCI spin–state splittings calculated from the extrapolated energies of individual states. Following the approach suggested in ref 49, the extrapolation error was estimated as the difference between the spin–state splitting calculated from the best available CIPSI energies and the one calculated from the extrapolated energies. This is treated as a measure of systematic error of each exFCI value. Note that CIPSI energies and resulting exFCI energies also have statistical uncertainties due to the usage of partly stochastic algorithm to efficiently evaluate the PT2 energy in QP2.[42] These statistical uncertainties are very small for CIPSI energies from individual iterations (see Supporting Information), but they increase by roughly one order of magnitude in the extrapolated energies due to the rules of error propagation. The resulting statistical uncertainties

Table 5: Extrapolated FCI (exFCI) Results. [a,b]

	exFCI [b]	σ [c]
$^{1,3}[FeHe_6]^{2+}$	-23.0 ± 0.8	0.4
$^{1,5}[FeHe_6]^{2+}$	-74.5 ± 0.5	0.3
$^{1,3}[FeH_6]^{4-}$	1 ± 6	2.0
$^{1,5}[FeH_6]^{4-}$	-5.2 ± 3.4	0.4
$^{1,5}[CoH_6]^{3-}$	30.9 ± 1.0	0.3
$^{2,6}[FeHe_6]^{3+}$	-125.0 ± 1.3	0.4
$^{3,5}[FeH_4]^{2-}$	-10.3 ± 1.7	0.6

[a] All values in kcal/mol. [b] The error bar is estimated extrapolation error, defined as the difference between the spin–state splitting calculated from the largest CIPSI wave functions and one calculated from the extrapolated energies. [c] Statistical uncertainty (one standard deviation) propagating from stochastic errors in CIPSI energies, calculated as $\sigma = \sqrt{\sigma_1^2 + \sigma_2^2}$, where are standard deviations of the extrapolated energies of individual states.

are reported as σ values in Table 5 and can also be seen as error bars adjacent to the dotted curves in the leftmost parts of Figures 2–5. As it becomes clear from Table 5, the statistical uncertainties (σ values) are always smaller than the extrapolation errors.[96]

Overall, this approach allows us to determine exFCI estimates with reasonably small extrapolation error for all but one investigated cases. This worst case is the singlet–triplet splitting in $[FeH_6]^{4-}$, for which the extrapolation error is 6 kcal/mol, preventing us from including this item in further analysis. For the remaining 5 items, we have obtained exFCI values reasonably looking error estimates: smaller than 1 kcal/mol for the singlet–triplet and singlet–quintet splittings in $[FeHe_6]^{2+}$, about 1 kcal/mol for the singlet–quintet splitting in $[CoH_6]^{3-}$, about 1.5 kcal/mol for the doublet–sextet splitting in $[FeHe_6]^{3+}$, about 2 kcal/mol for the triplet–quintet splitting in $[FeH_4]^{2-}$, and about 3.5 kcal/mol for the singlet–quintet splitting in $[FeH_6]^{4-}$. The latter largest error estimate is clearly related to the computational difficulty of the $^{1,5}[FeH_6]^{4-}$ energy difference and its great variability with the choice of method (cf the largest $\sigma_{\Delta E}$ value in Table 3).

3.6 Benchmarking Against exFCI

The above determined exFCI spin–state splittings (cf Table 5) are now taken as reference values for benchmarking the accuracy of approximate wave function methods. The small basis aT/D′ basis set is used throughout and (as discussed above) only the following energies are considered: $^{1,3}[Fe^{II}He_6]^{2+}$, $^{1,5}[Fe^{II}He_6]^{2+}$, $^{1,5}[Fe^{II}H_6]^{4-}$, $^{1,5}[Co^{III}H_6]^{3-}$, $^{2,6}[Fe^{III}He_6]^{3+}$, and $^{3,5}[Fe^{II}H_4]^{2-}$.

Table 6 reports deviations of calculated spin–state energetics from the exFCI reference value. For clarity, the table cells are color-mapped by deviation from the reference interval taking into account the error bar of the reference value: for deviation within the error bars, the cell is left white; for positive/negative deviation beyond the error bars, the cell is colored red/blue, respectively, with the intensity proportional to the magnitude of the deviation. In addition to methods already tested before, i.e., CASPT2, MRCI+Q, CCSD(T) and PBE-CCSD(T), the comparison now also include CASPT2/CC,[14] NEVPT2,[97,98] CASPT3,[99] more variants of MRCI and a variety of CC methods with up to approximate quadruples.

We start the discussion of data in Table 6 from multireference perturbation theory approaches (CASPT2, CASPT2/CC, NEVPT2, CASPT3). The present results confirm the known tendency of CASPT2 calculations (with the standard choice of active space) to overstabilize higher-spin states.[24,25,73] For the studied models, the overstabilization errors are sized up to 9 kcal/mol in magnitude when using the default formulation with IPEA shift of 0.25 hartree.[100] The original formulation of the CASPT2 method without the IPEA shift leads to even larger errors. The CASPT3 method, even if computationally much more expensive than CASPT2, yields comparable errors. Thus, the CASPT2.5 method (which comes down to averaging the CASPT2 and CASPT3 results), previously recommended based on atomic benchmark data,[16] would not work well for the presently investigated complexes. The negative errors observed in the CASPT2 calculations are systematically reduced by the hybrid CASPT2/CC method,[14] which was proposed in the literature for exactly this purpose. However, the reduction of errors is far from being perfect, particularly for $^{1,5}[FeH_6]^{4-}$ and $^{2,6}[FeHe_6]^{3+}$, where the higher-spin state is still overstabilized by several kcal/mol. The NEVPT2 method performs best, yielding deviations with respect to the

Table 6: Deviations of Calculated Spin–State Splittings from the exFCI Reference Values. [a,b].

	$^{1,3}[FeHe_6]^{2+}$	$^{1,5}[FeHe_6]^{2+}$	$^{1,5}[FeH_6]^{4-}$	$^{1,5}[CoH_6]^{3-}$	$^{2,6}[FeHe_6]^{3+}$	$^{3,5}[FeH_4]^{2-}$
CASPT2(noIPEA)	−4.9	−11.8	−16.7	−13.4	−10.0	−7.3
CASPT2	−3.1	−9.3	−12.1	−4.9	−9.1	−5.4
CASPT2/CC	−0.1	−3.6	−8.2	−1.4	−6.7	−4.1
NEVPT2	0.4	−1.6	1.1	0.6	−1.7	1.6
CASPT3	0.6	−1.3	−10.0	−5.6	[c]	−4.2
MRCI	1.0	−1.5	−12.9	−6.5	−4.8	−6.4
MRCI+Q(RDC)	1.0	−0.7	−8.6	−3.8	−2.8	−3.5
MRCI+Q(DSS)	1.0	−0.6	−7.5	−3.1	−2.4	−2.9
MRCI+Q(PC)	1.0	−0.7	−8.1	−3.5	−2.7	−3.3
ACPF	[c]	[c]	−6.5	[c]	[c]	[c]
AQCC	[c]	[c]	−8.7	[c]	[c]	[c]
MP2	−2.1	−12.4	−32.1	−24.8	−23.6	−19.4
CCSD	−0.1	−5.8	−17.7	−16.5	−11.6	−10.3
DCSD	−0.3	−4.7	−1.5	−0.8	−8.3	−4.1
CCSD(T)	0.4	−3.1	−3.1	2.3	−6.5	−3.0
PBE-CCSD(T)	0.5	−3.0	6.8	2.8	−4.7	−2.2
UHF-CCSD(T)	0.3	−3.4	−3.3	2.2	−6.9	−2.9
UHF-CCSD[T]	0.3	−3.3	9.7	34.9	−6.4	2.2
UHF-CCSD(T)$_\Lambda$	0.3	−3.5	−7.5	4.1	−7.3	−4.4
UHF-CCSDT	−0.5	−2.0	1.1	−1.6	−2.9	−1.5
UHF-CCSDT(Q)	−0.4	−1.4	16.6	4.6	−1.4	1.2
UHF-CCSDT[Q]	−0.3	−1.8	−1.9	−8.7	−2.8	−1.9
UHF-CCSDT(Q)$_\Lambda$	−0.3	−1.4	3.4	−0.8	−1.4	−0.3

[a]Values in kcal/mol. [b]All calculations performed using aT/D′ basis set. [c]Calculations not performed.

exFCI values no greater than 2 kcal/mol in magnitude (both positive and negative deviations are observed). In fact, NEVPT2 performs comparably or even better than variational MRCI+Q (see below) and appears to be the most accurate method of all benchmarked in Table 6. Interestingly, the presently observed good performance of NEVPT2 disagrees with much larger errors observed in the NEVPT2 spin–state energetics of realistic TM complexes[24] and metallocenes,[25] for which the reference values were derived from experimental data. The origin of this discrepancy is not entirely clear, but is presumably related to larger molecule size of the complexes studied in refs 24 and 25, and hence more complicated character of their correlation effects than in presently studied hydride/helium small models.

The performance of the MRCI+Q method is particularly worth of attention. The MRCI+Q results are provided in Table 6 for several choices of the size-consistency correction (DSS, RDC, PC; see Computational Details) in addition to uncorrected MRCI results. Different choices of the size-consistency corrections give rather similar results, whereas differences between uncorrected MRCI and MRCI+Q values range from negligible up to 3 kcal/mol. The MRCI+Q method gives a nearly perfect agreement with the exFCI reference values for the helium model ($^{1,3}[Fe^{II}He_6]^{2+}$, $^{1,5}[Fe^{II}He_6]^{2+}$), but features larger discrepancies for hydride models, particularly for the $^{1,5}[Fe^{II}H_6]^{2+}$ splitting. Interestingly, the problem with the accuracy of the MRCI+Q for this particularly challenging energy difference is not solved by switching to ACPF or AQCC, which are two size-consistent generalizations of the MRCI: both ACPF and AQCC give similar results as MRCI+Q (identical to within 1.5 kcal/mol), and all three significantly deviate from the exFCI reference value. Overall, the present results suggest that the MRCI+Q (with singles and doubles beyond the active space and the standard choice of active space) is not necessarily a very accurate method for spin–state energetics, although it might be very accurate in certain cases. This observation agrees with the experience gained in the previous study of spin–state energetics for octahedral complexes,[24] where also large errors, up to several kcal/mol in magnitude, were observed in the MRCI+Q calculations, particularly with the standard (RDS) size-consistency correction. In larger complexes the differences between different choices of the correction are also more pronounced[24]

than in the present set of hydride/helium models, which is presumably related to growing deviations from size-consistency, being only partly restored within the MRCI+Q approach, in the case of larger complexes.

Proceeding now to single-reference methods benchmarked in Table 6, we start from the simplest MP2 and CCSD methods. As might be expected, they both lead to significant errors, often greater in magnitude than 10 kcal/mol. (The only exception is singlet–triplet splitting for $[FeHe_6]^{2+}$, which is computed relatively accurately by most of the benchmarked methods, including CCSD.) The negative errors observed with these methods indicate overstabilization of higher-spin states due to underestimation of correlation effects.[87,101,102] Interestingly, however, the distinguishable cluster (DC) with singles and doubles (DCSD) usually leads to significantly smaller negative errors than in analogous calculations at the CCSD level. With the "gold standard" CCSD(T) method, the energy differences are usually within 3 kcal/mol from the exFCI reference values and both positive and negative deviations are observed. The largest CCSD(T)'s error of −6.5 kcal/mol occurs for the doublet–sextet splitting of $[FeHe_6]^{3+}$. This is presumably rooted in a very considerable multiconfigurational character for the doublet state (%MC diagnostic of 29%), whereas the sextet state is essentially single-configurational (%MC diagnostic of 0.6%).

The next interesting question is the effect of switching from canonical HF to DFT (PBE) orbitals in the reference Slater determinant, i.e., CCSD(T) vs PBE-CCSD(T) results in Table 6. It turns out that the effect is very limited for $[FeHe_6]^{2+}$ and $[CoH_6]^{3-}$ models, but more pronounced for other models, particularly for $[Fe^{II}H_6]^{4-}$. In all presently investigated cases the use of PBE orbitals leads to larger (i.e., more positive or less negative) spin–state splittings. The use of PBE orbitals is beneficial in some cases ($^{2,6}[FeHe_6]^{2+}$, $^{3,5}[FeH_4]^{2+}$), but neither of the two choices of reference orbitals is systematically better for all the energy differences considered simultaneously. This observation aligns with the study of small systems by Benedek et al.[38] and with the experience gained for TM complexes with larger ligands, showing that the optimal choice of reference orbitals in CCSD(T) calculations of spin–state energetics is still an open question (see also discussion in refs 12 and 87, and references therein).

The MP2, CC and DC results discussed so far were based on the ROHF-type Slater determinant. However, Table 6 also includes CC results based on a UHF-type Slater determinant, which are identified by the "UHF-" prefix. (The latter set of calculations was performed using the MRCC software, to enable fully iterative treatment of the triples and approximate treatment of quadruples. The switch from the ROHF to the UHF reference is motivated by technical reasons, i.e., limitations of the Molpro/MRCC interface.) The corresponding ROHF-based CCSD(T) and UHF-CCSD(T) results are identical to within 0.4 kcal/mol. This was to be expected as the UHF spin contamination is very small for the presently investigated systems (cf Table S9, Supporting Information).

Using the UHF reference, different formulations of the perturbative triples correction are considered: CCSD[T],[103] CCSD(T)[104] CCSD(T)$_\Lambda$,[105,106] as well as full CCSDT.[107] Note that although the CCSD(T) formulation is usually preferred and it benefits from partial error cancellations between the post-(T) triples and higher excitations,[88,108,109] the CCSD[T] formulation has been observed to yield results closer to full CCSDT for intermolecular interaction energies.[110] For the presently studied models, the UHF-CCSD(T) formulation performs slightly better than UHF-CCSD(T)$_\Lambda$ and significantly better than UHF-CCSD[T], as the latter one leads to very large errors for $[FeH_6]^{4-}$ and $[CoH_6]^{3-}$. The UHF-CCSDT method with iterative treatment of the triples produce results that differ from the corresponding UHF-CCSD(T) results by up to 4 kcal/mol. The difference are usually positive (i.e., indicating a greater stabilization of the lower-spin state with the UHF-CCSDT than with UHF-CCSD(T) method), except for the $^{1,5}[CoH_6]^{3-}$ splitting, for which the opposite behavior is observed. The UHF-CCSDT spin–state splittings agree with the exFCI reference values to within 3 kcal/mol and are consistently more accurate than the UHF-CCSD(T) spin–state splittings (the only exception is $^{1,3}[FeHe_6]^{2+}$, for which the errors of the two methods are very small and practically identical).

The analogous CC methods are considered for approximate treatment of quadruple excitations:[111,112] CCSDT[Q], CCSDT(Q), and CCSDT(Q)$_\Lambda$. The results obtained are highly intriguing. With the UHF-CCSDT(Q) method, the computed spin–state splittings are usually very close to the corresponding exFCI reference values, but a very significant discrepancy (of nearly 17 kcal/mol)

is observed for the $^{1,5}[FeH_6]^{4-}$ splitting. It thus appears that the CCSDT(Q) value is completely unreliable due to problems with perturbative treatment of quadruple excitations in this particular molecule, containing very covalent Fe^{II}–ligand bond and significantly diffused negative charge on the ligands. The origin of this error is not clear, but it may be analogous to known problems with perturbatively-corrected CC calculations for multiple bond dissociation curves, for example in stretched N_2.[28,113] The UHF-CCSDT(Q) method also leads to considerable error of nearly 5 kcal/mol for the $^{1,5}[CoH_6]^{3-}$ splitting. With the UHF-CCSDT[Q] method, the error on the $^{1,5}[FeH_6]^{4-}$ splitting is reduced to only 2 kcal/mol (i.e., below the uncertainty of this reference value; cf Table 5), but the error on the $^{1,5}[CoH_6]^{3-}$ splitting grows to about 9 kcal/mol. Finally, with the UHF-CCSDT(Q)$_\Lambda$ method, all discrepancies with respect to the exFCI reference values are within 2 kcal/mol, except for the $^{1,5}[FeH_6]^{4-}$ splitting, for which the observed discrepancy is somewhat larger, 3.4 kcal/mol, yet still comparable to the uncertainty of the reference value. Thus, based on the present benchmark, the best performing CC method with approximate quadruples seems to be UHF-CCSDT(Q)$_\Lambda$, whereas neither UHF-CCSDT(Q) nor UHF-CCSDT[Q] can be safely recommended due to the sizable maximum errors observed for $[FeH_6]^{3-}$ and $[CoH_6]^{3-}$.

It remains unknown whether similar problems with the CCSDT(Q)'s accuracy can be also observed in larger TM complexes. Post-(T) calculations are very rarely performed for TM complexes due to their prohibitively high computational cost. One example of such calculations was given in our study of the quartet–sextet splitting for $[Fe(H_2O)_6]^{3+}$,[114] where the CCSD(T) and CCSDT(Q) relative energies computed using small basis set were shown to agree to within 1 kcal/mol. Bross *et al.*[115] compared the performance of CCSDT(Q) and CCSDT(Q)$_\Lambda$ with respect to full CCSDTQ for atomization energies of 8 small molecules (diatomic or triatomic) containing one TM atom. For this, they also found that the CCSDT(Q)$_\Lambda$ formulation performs better than the CCSDT(Q) one, although the discrepancies between the two formulations were within 3 kcal/mol, therefore much smaller than in the presently studied cases of $[FeH_6]^{4-}$ and $[CoH_6]^{3-}$.

4 Conclusions

In this work, a set of small complexes with hydride and helium ligands has been presented to deliver computationally convenient, highly reduced models for the challenging problem of first-row TM spin–state energetics. It has been demonstrated that these models, despite their enormous simplicity, capture essential aspects of the electronic structure found in larger TM complexes with σ-donor ligand, whereas their spin–state splittings feature comparable method-dependence as in realistic complexes. After carefully determining the basis set limits for a few selected methods and studying transferability of the basis set incompleteness errors, a small basis set has been proposed for further benchmarking of wave function theory methods. The reference exFCI spin–state splittings have been obtained from CIPSI calculations with up to 10^9 determinants in the variational CI part. The benchmarking results show that it is possible to reproduce the exFCI reference values using both multireference and single-reference approaches, among which the NEVPT2 and CCSDT(Q)$_\Lambda$ methods performed best. The gold-standard CCSD(T) method produced deviations from the reference values which were in most cases about 3 kcal/mol or smaller, with the exception of the doublet–sextet splitting in $[FeHe_6]^{3+}$, where more than twice larger error was observed and tentatively attributed to significant multiconfigurational character in the doublet state. Accurate determination of the singlet–quintet splittings in $[FeH_6]^{4-}$ and $[CoH_6]^{3-}$, in view of the slow convergence of the CIPSI calculations, large errors in MRCI+Q, ACPF and AQCC results and considerable variation of the higher-order CC results, appears to be a particularly challenging problem, perhaps comparable in the difficulty to the well known chromium dimer.[42,43,116–118] Overall, the presented hydride and helium models of TM complexes make up a challenging benchmark set, quite distinct from TM diatomics or bare ions so extensively studied in the literature, that may be worth of further attention in the context of developing novel wave function methods.

Supporting Information Available

Outer-core (Δ3s3p) correlation corrections, comparison of alternative CBS extrapolations, spin–state energetics in smaller basis sets, detailed CIPSI results, sample Molpro input files.

Acknowledgement

The author is grateful to Prof. Emmanuel Giner and Prof. Anthony Scemama (Paul Sabatier University Toulouse III) for valuable discussion and advice on the CIPSI calculations in Quantum Package software. This research was supported by National Science Centre, Poland, under grant no. 2017/26/D/ST4/00774. Part of the study was carried out using research infrastructure purchased with the funds of the European Union in the framework of the Smart Growth Operational Programme, Measure 4.2; Grant No. POIR.04.02.00-00-D001/20, "ATOMIN 2.0 - ATOMic scale science for the INnovative economy." We gratefully acknowledge Poland's high-performance computing infrastructure PLGrid (HPC Centers: ACK Cyfronet AGH) for providing computer facilities and support within computational grants no. PLG/2023/016069 and PLG/2024/016907.

References

(1) Swart, M.; Güell, M.; Solá, M. In *Quantum Biochemistry*; Matta, C. F., Ed.; Wiley-Blackwell, 2010; Vol. 2; Chapter 19, pp 551–583.

(2) Harvey, J. N. Spin-forbidden reactions: computational insight into mechanisms and kinetics. *WIREs Comput. Mol. Sci.* **2014**, *4*, 1–14.

(3) Swart, M., Costas, M., Eds. *Spin States in Bioinorganic and Inorganic Chemistry: Influence on Structure and Reactivity*; Wiley, 2015.

(4) Swart, M.; Gruden, M. Spinning around in Transition-Metal Chemistry. *Acc. Chem. Res.* **2016**, *49*, 2690–2697.

(5) Kepp, K. P. In *Transition Metals in Coordination Environments: Computational Chemistry and Catalysis Viewpoints*; Broclawik, E., Borowski, T., Radoń, M., Eds.; Challenges and Advances in Computational Chemistry and Physics; Springer International Publishing: Cham, 2019; Vol. 29; Chapter 1, pp 1–33.

(6) Swart, M. *New Directions in the Modeling of Organometallic Reactions*; Topics in Organometallic Chemistry; Springer: Cham, 2020; Vol. 67; pp 191–226.

(7) Harvey, J. N. On the accuracy of density functional theory in transition metal chemistry. *Annu. Rep. Prog. Chem., Sect. C: Phys. Chem.* **2006**, *102*, 203–226.

(8) Costas, M.; Harvey, J. N. Spin states: Discussion of an open problem. *Nature Chemistry* **2013**, *5*, 7–9.

(9) Swart, M. Spin States of (Bio)inorganic Systems: Successes and Pitfalls. *Int. J. Quantum Chem.* **2013**, *113*, 2–7.

(10) Feldt, M.; Phung, Q. M. Ab Initio Methods in First-Row Transition Metal Chemistry. *Eur. J. Inorg. Chem.* **2022**, e202200014.

(11) Radoń, M. In *Advances in Inorganic Chemistry*; van Eldik, R., Puchta, R., Eds.; Academic Press, 2019; Vol. 73; Chapter 7, pp 221–264.

(12) Radoń, M. Benchmarks for transiton metal spin–state energetics: Why and how to employ experimental reference data? *Phys. Chem. Chem. Phys.* **2023**, *25*, 30800–30820.

(13) Römer, A.; Hasecke, L.; Blöchl, P.; Mata, R. A. A Review of Density Functional Models for the Description of Fe(II) Spin-Crossover Complexes. *Molecules* **2020**, *25*, 5176.

(14) Phung, Q. M.; Feldt, M.; Harvey, J. N.; Pierloot, K. Towards Highly Accurate Spin State Energetics in First-Row Transition Metal Complexes: A Combined CASPT2/CC Approach. *J. Chem. Theory Comput.* **2018**, *14*, 2446–2455.

(15) Song, S.; Kim, M.-C.; Sim, E.; Benali, A.; Heinonen, O.; Burke, K. Benchmarks and Reliable DFT Results for Spin Gaps of Small Ligand Fe(II) Complexes. *J. Chem. Theory Comput.* **2018**, *14*, 2304–2311.

(16) Zhang, D.; Truhlar, D. G. Spin Splitting Energy of Transition Metals: A New, More Affordable Wave Function Benchmark Method and Its Use to Test Density Functional Theory. *J. Chem. Theory Comput.* **2020**, *16*, 4416–4428.

(17) Mariano, L. A.; Vlaisavljevich, B.; Poloni, R. Improved Spin-State Energy Differences of Fe(II) Molecular and Crystalline Complexes via the Hubbard U-Corrected Density. *J. Chem. Theory Comput.* **2021**, *17*, 2807–2816.

(18) Drosou, M.; Mitsopoulou, C. A.; Pantazis, D. A. Reconciling Local Coupled Cluster with Multireference Approaches for Transition Metal Spin-State Energetics. *J. Chem. Theory Comput.* **2022**, *18*, 3538–3548.

(19) Reimann, M.; Kaupp, M. Spin-State Splittings in 3d Transition-Metal Complexes Revisited: Benchmarking Approximate Methods for Adiabatic Spin-State Energy Differences in Fe(II) Complexes. *J. Chem. Theory Comput.* **2022**, *28*, 7442–7456.

(20) Reimann, M.; Kaupp, M. Spin-State Splittings in 3d Transition-Metal Complexes Revisited: Toward a Reliable Theory Benchmark. *J. Chem. Theory Comput.* **2023**, *19*, 97–108.

(21) Kepp, K. P. Theoretical Study of Spin Crossover in 30 Iron Complexes. *Inorg. Chem.* **2016**, *55*, 2717–2727.

(22) Cirera, J.; Via-Nadal, M.; Ruiz, E. Benchmarking Density Functional Methods for Calculation of State Energies of First Row Spin-Crossover Molecules. *Inorg. Chem.* **2018**, *57*, 14097–14105.

(23) Verma, P.; Varga, Z.; Klein, J. E. M. N.; Cramer, C. J.; Que, L.; Truhlar, D. G. Assessment of

electronic structure methods for the determination of the ground spin states of Fe(II), Fe(III) and Fe(IV) complexes. *Phys. Chem. Chem. Phys.* **2017**, *19*, 13049–13069.

(24) Radoń, M. Benchmarking quantum chemistry methods for spin-state energetics of iron complexes against quantitative experimental data. *Phys. Chem. Chem. Phys.* **2019**, *21*, 4854–4870.

(25) Drabik, G.; Szklarzewicz, J.; Radoń, M. Spin–state energetics of metallocenes: How do best wave function and density functional theory results compare with the experimental data? *Phys. Chem. Chem. Phys.* **2021**, *23*, 151–172.

(26) Radoń, M.; Drabik, G.; Hodorowicz, M.; Szklarzewicz, J. Performance of Quantum Chemistry Methods for Benchmark Set of Spin–State Energetics Derived from Experimental Data of 17 Transition Metal Complexes (SSE17). 2024.

(27) Mata, R. A.; Suhm, M. A. Benchmarking Quantum Chemical Methods: Are We Heading in the Right Direction? *Angew. Chem. Int. Ed.* **2017**, *56*, 11011–11018.

(28) Bartlett, R. J.; Musial, M. Coupled-cluster theory in quantum chemistry. *Rev. Mod. Phys.* **2007**, *79*, 291–352.

(29) Pierloot, K. The CASPT2 Method in Inorganic Electronic Spectroscopy: From Ionic Transition Metal to Covalent Actinide Complexes. *Mol. Phys.* **2003**, *101*, 2083–2094.

(30) Roca-Sanjuán, D.; Aquilante, F.; Lindh, R. Multiconfiguration second-order perturbation theory approach to strong electron correlation in chemistry and photochemistry. *Wiley Interdisciplinary Reviews: Computational Molecular Science* **2012**, *2*, 585–603.

(31) Szalay, P. G.; Müller, T.; Gidofalvi, G.; Lischka, H.; Shepard, R. Multiconfiguration Self-Consistent Field and Multireference Configuration Interaction Methods and Applications. *Chem. Rev.* **2012**, *112*, 108–181.

(32) Rudshteyn, B.; Weber, J. L.; Coskun, D.; Devlaminck, P. A.; Zhang, S.; Reichman, D. R.; Shee, J.; Friesner, R. A. Calculation of Metallocene Ionization Potentials via Auxiliary Field Quantum Monte Carlo: Toward Benchmark Quantum Chemistry for Transition Metals. *J. Chem. Theory Comput.* **2022**, *18*, 2845–2862.

(33) Vitale, E.; Li Manni, G.; Alavi, A.; Kats, D. FCIQMC-Tailored Distinguishable Cluster Approach: Open-Shell Systems. *J. Chem. Theory Comput.* **2022**, *18*, 3427–3437.

(34) Xu, X.; Zhang, W.; Tang, M.; Truhlar, D. G. Do Practical Standard Coupled Cluster Calculations Agree Better than Kohn–Sham Calculations with Currently Available Functionals When Compared to the Best Available Experimental Data for Dissociation Energies of Bonds to 3d Transition Metals? *J. Chem. Theory Comput.* **2015**, *11*, 2036–2052.

(35) Fang, Z.; Vasiliu, M.; Peterson, K. A.; Dixon, D. A. Prediction of Bond Dissociation Energies/Heat of Formation for Diatomic Transition metal Compounds: CCSD(T) Works. *J. Chem. Theory Comput.* **2017**, *13*, 1057–1066.

(36) Aoto, Y. A.; de Lima Batista, A. P.; Köhn, A.; de Oliveira-Filho, A. G. S. How To Arrive at Accurate Benchmark Values for Transition Metal Compounds: Computation or Experiment? *J. Chem. Theory Comput.* **2017**, *13*, 5291–5316.

(37) Feldt, M.; Phung, Q. M.; Pierloot, K.; Mata, R. A.; Harvey, J. N. Limits of Coupled-Cluster Calculations for Non-Heme Iron Complexes. *J. Chem. Theory Comput.* **2019**, *15*, 922–937.

(38) Benedek, Z.; Timár, P.; Szilvási, T.; Barcza, G. Sensitivity of coupled cluster electronic properties on the reference determinant: Can Kohn-Sham orbitals be more beneficial than Hartree-Fock orbitals? *J Comput Chem* **2022**, *43*, 2103–2120.

(39) Gdanitz, R. J.; Ahlrichs, R. The averaged coupled-pair functional (ACPF): A size-extensive modification of MR CI(SD). *Chemical Physics Letters* **1988**, *143*, 413–420.

(40) Szalay, P. G.; Bartlett, R. J. Multi-reference averaged quadratic coupled-cluster method: a size-extensive modification of multi-reference CI. *Chemical Physics Letters* **1993**, *214*, 481–488.

(41) Huron, B.; Malrieu, J. P.; Rancurel, P. Iterative perturbation calculations of ground and excited state energies from multiconfigurational zeroth-order wavefunctions. *J. Chem. Phys.* **1973**, *58*, 5745–5759.

(42) Garniron, Y.; Scemama, A.; Loos, P.-F.; Caffarel, M. Hybrid stochastic-deterministic calculation of the second-order perturbative contribution of multireference perturbation theory. *J. Chem. Phys.* **2017**, *147*, 034101.

(43) Garniron, Y.; Applencourt, T.; Gasperich, K.; Benali, A.; Ferté, A.; Paquier, J.; Pradines, B.; Assaraf, R.; Reinhardt, P.; Toulouse, J.; Barbaresco, P.; Renon, N.; David, G.; Malrieu, J.-P.; Véril, M.; Caffarel, M.; Loos, P.-F.; Giner, E.; Scemama, A. Quantum Package 2.0: An Open-Source Determinant-Driven Suite of Programs. *J. Chem. Theory Comput.* **2019**, *15*, 3591–3609.

(44) Li, J.; Otten, M.; Holmes, A. A.; Sharma, S.; Umrigar, C. J. Fast semistochastic heat-bath configuration interaction. *J. Chem. Phys.* **2018**, *149*, 214110.

(45) Chilkuri, V. G.; Neese, F. Comparison of Many-Particle Representations for Selected Configuration Interaction: II. Numerical Benchmark Calculations. *J. Chem. Theory Comput.* **2021**, *17*, 2868–2885.

(46) Zimmerman, P. M. Incremental full configuration interaction. *J. Chem. Phys.* **2017**, *146*, 104102.

(47) Tubman, N. M.; Lee, J.; Takeshita, T. Y.; Head-Gordon, M.; Whaley, K. B. A deterministic alternative to the full configuration interaction quantum Monte Carlo method. *J. Chem. Phys.* **2016**, *145*, 044112.

(48) Loos, P.-F.; Scemama, A.; Blondel, A.; Garniron, Y.; Caffarel, M.; Jacquemin, D. A Mountaineering Strategy to Excited States: Highly Accurate Reference Energies and Benchmarks. *J. Chem. Theory Comput.* **2018**, *14*, 4360–4379.

(49) Loos, P.-F.; Lipparini, F.; Boggio-Pasqua, M.; Scemama, A.; Jacquemin, D. A Mountaineering Strategy to Excited States: Highly Accurate Energies and Benchmarks for Medium Sized Molecules. *J. Chem. Theory Comput.* **2020**, *16*, 1711–1741.

(50) Caffarel, M.; Giner, E.; Scemama, A.; Ramírez-Solís, A. Spin Density Distribution in Open-Shell Transition Metal Systems: A Comparative Post-Hartree-Fock, Density Functional Theory, and Quantum Monte Carlo Study of the CuCl2 Molecule. *J. Chem. Theory Comput.* **2014**, *10*, 5286–5296.

(51) Giner, E.; Angeli, C. Metal-ligand delocalization and spin density in the $CuCl_2$ and $[CuCl_4]^{2-}$ molecules: Some insights from wave function theory. *J. Chem. Phys.* **2015**, *143*, 124305.

(52) Giner, E.; Tew, D. P.; Garniron, Y.; Alavi, A. Interplay between Electronic Correlation and Metal-Ligand Delocalization in the Spectroscopy of Transition Metal Compounds: Case Study on a Series of Planar Cu2+ Complexes. *J. Chem. Theory Comput.* **2018**, *14*, 6240–6252.

(53) Scemama, A.; Garniron, Y.; Caffarel, M.; Loos, P.-F. Deterministic Construction of Nodal Surfaces within Quantum Monte Carlo: The Case of FeS. *J. Chem. Theory Comput.* **2018**, *14*, 1395–1402.

(54) Yvon, K.; Renaudin, G. In *Encyclopedia of Inorganic and Bioinorganic Chemistry*; Scott, R., Ed.; Wiley, 2006.

(55) Cohen, A. J.; Mori-Sánchez, P.; Yang, W. Challenges for Density Functional Theory. *Chem. Rev.* **2012**, *112*, 289–320.

(56) Werner, H.-J.; Knowles, P. J.; Knizia, G.; Manby, F. R.; Schütz, M.; Celani, P.; Györffy, W.; Kats, D.; Korona, T.; Lindh, R.; Mitrushenkov, A.; Rauhut, G.; Shamasundar, K. R.; Adler, T. B.; Amos, R. D.; Bernhardsson, A.; Berning, A.; Cooper, D. L.; Deegan, M. J. O.; Dobbyn, A. J.; Eckert, F.; Goll, E.; Hampel, C.; Hesselmann, A.; Hetzer, G.; Hrenar, T.; Jansen, G.; Köppl, C.; Liu, Y.; Lloyd, A. W.; Mata, R. A.; May, A. J.; McNicholas, S. J.; Meyer, W.; Mura, M. E.; Nicklass, A.; O'Neill, D. P.; Palmieri, P.; Peng, D.; Pflüger, K.; Pitzer, R.; Reiher, M.; Shiozaki, T.; Stoll, H.; Stone, A. J.; Tarroni, R.; Thorsteinsson, T.; Wang, M. MOLPRO, version 2015.1, a package of ab initio programs. 2015; see `http://www.molpro.net`.

(57) MRCC, v.2015, a quantum chemical program suite written by M. Kállay, Z. Rolik, I. Ladjánszki, L. Szegedy, B. Ladóczki, J. Csontos, and B. Kornis. See also Z. Rolik, L. Szegedy, I. Ladjánszki, B. Ladóczki, and M. Kállay, *J. Chem. Phys.* **139**, 094105 (2013), as well as: `www.mrcc.hu`.

(58) Aquilante, F.; Autschbach, J.; Baiardi, A.; Battaglia, S.; Borin, V. A.; Chibotaru, L. F.; Conti, I.; De Vico, L.; Delcey, M.; Fdez. Galván, I.; Ferré, N.; Freitag, L.; Garavelli, M.; Gong, X.; Knecht, S.; Larsson, E. D.; Lindh, R.; Lundberg, M.; Malmqvist, P. Å.; Nenov, A.; Norell, J.; Odelius, M.; Olivucci, M.; Pedersen, T. B.; Pedraza-González, L.; Phung, Q. M.; Pierloot, K.; Reiher, M.; Schapiro, I.; Segarra-Martí, J.; Segatta, F.; Seijo, L.; Sen, S.; Sergentu, D.-C.; Stein, C. J.; Ungur, L.; Vacher, M.; Valentini, A.; Veryazov, V. Modern quantum chemistry with [Open]Molcas. *J. Chem. Phys.* **2020**, *152*, 214117.

(59) Knowles, P. J.; Hampel, C.; Werner, H.-J. Coupled cluster theory for high spin, open shell reference wave functions. *J. Chem. Phys.* **1993**, *99*, 5219–5227.

(60) Perdew, J. P.; Burke, K.; Ernzerhof, M. Generalized Gradient Approximation Made Simple. *Phys. Rev. Lett.* **1996**, *77*, 3865–3868.

(61) Pierloot, K. Transition Metals Compounds: Outstanding Challenges for Multiconfigurational Methods. *Int. J. Quantum Chem.* **2011**, *111*, 3291–3301.

(62) Sousa, C.; de Graaf, C. *Spin States in Biochemistry and Inorganic Chemistry*; Wiley, 2015; pp 35–57.

(63) Shamasundar, K. R.; Knizia, G.; Werner, H.-J. A new internally contracted multi-reference configuration interaction method. *J. Chem. Phys.* **2011**, *135*, 054101.

(64) Celani, P.; Werner, H.-J. Multireference perturbation theory for large restricted and selected active space reference wave functions. *J. Chem. Phys.* **2000**, *112*, 5546–5557.

(65) Werner, H.; Knowles, P. J. An efficient internally contracted multiconfiguration-reference configuration interaction method. *J. Chem. Phys.* **1988**, *89*, 5803–5814.

(66) Lawson Daku, L. M.; Aquilante, F.; Robinson, T. W.; Hauser, A. Accurate Spin-State Energetics of Transition Metal Complexes. 1. CCSD(T), CASPT2, and DFT Study of $[M(NCH)_6]^{2+}$ (M = Fe, Co). *J. Chem. Theory Comput.* **2012**, *8*, 4216–4231.

(67) Flöser, B. M.; Guo, Y.; Riplinger, C.; Tuczek, F.; Neese, F. Detailed Pair Natural Orbital-based Coupled Cluster Studies of Spin Crossover Energetics. *J. Chem. Theory Comput.* **2020**, *16*, 2224–2235.

(68) Helgaker, T.; Klopper, W.; Koch, H.; Noga, J. Basis-set convergence of correlated calculations on water. *J. Chem. Phys.* **1997**, *106*, 9639–9646.

(69) Knowles, P. J.; Handy, N. C. A determinant based full configuration interaction program. *Computer Physics Communications* **1989**, *54*, 75–83.

(70) Hermann, G.; Pohl, V.; Tremblay, J. C.; Paulus, B.; Hege, H.-C.; Schild, A. ORBKIT: A modular python toolbox for cross-platform postprocessing of quantum chemical wavefunction data. *J. Comput. Chem.* **2016**, *37*, 1511–1520.

(71) Radoń, M.; Brocławik, E. In *Computational methods to study the structure and dynamics of biomolecules and biomolecular processes – from bioinformatics to molecular quantum mechanics.*; Liwo, A., Ed.; Springer series on Bio-/Neuroinformatics, vol. 1; Springer: Berlin Heidelberg, 2014; pp 711–782.

(72) Radoń, M. Spin-State Energetics of Heme-Related Models from DFT and Coupled Cluster Calculations. *J. Chem. Theory Comput.* **2014**, *10*, 2306–2321.

(73) Pierloot, K.; Phung, Q. M.; Domingo, A. Spin State Energetics in First-Row Transition Metal Complexes: Contribution of (3s3p) Correlation and its Description by Second-Order Perturbation Theory. *J. Chem. Theory Comput.* **2017**, *13*, 537–553.

(74) Lee, T. J.; Taylor, P. R. A diagnostic for determining the quality of single-reference electron correlation methods. *Int. J. Quantum Chem.* **1989**, *36*, 199–207.

(75) Janssen, C. L.; Nielsen, I. M. B. New diagnostics for coupled-cluster and Møller-Plesset perturbation theory. *Chem. Phys. Lett.* **1998**, *290*, 423–430.

(76) Lee, T. J.; Scuseria, G. E. In *Quantum Mechanical Electronic Structure Calculations with Chemical Accuracy*; Langhoff, S. R., Ed.; Springer: Dordrecht, 1995; pp 47–108.

(77) Aðalsteinsson, H. M.; Bjornsson, R. Ionization energies of metallocenes: a coupled cluster study of cobaltocene. *Phys. Chem. Chem. Phys.* **2023**, *25*, 4570–4587.

(78) Jiang, W.; DeYonker, N. J.; Wilson, A. K. Multireference Character for 3d Transition-Metal-Containing Molecules. *J. Chem. Theory Comput.* **2012**, *8*, 460–468.

(79) Tishchenko, O.; Zheng, J.; Truhlar, D. G. Multireference Model Chemistries for Thermochemical Kinetics. *J. Chem. Theory Comput.* **2008**, *4*, 1208–1219.

(80) Sprague, M. K.; Irikura, K. K. Quantitative estimation of uncertainties from wavefunction diagnostics. *Theor. Chem. Acc.* **2014**, *133*, 1544.

(81) Fogueri, U. R.; Kozuch, S.; Karton, A.; Martin, J. M. L. A simple DFT-based diagnostic for nondynamical correlation. *Theor. Chem. Acc.* **2012**, *132*, 1291.

(82) Stępniewski, A.; Radoń, M.; Góra-Marek, K.; Broclawik, E. Ammonia-modified Co(II) sites in zeolites: spin and electron density redistribution through the Co^{II} –NO bond. *Phys. Chem. Chem. Phys.* **2016**, *18*, 3716–3729.

(83) Schultz, N. E.; Zhao, Y.; Truhlar, D. G. Density Functionals for Inorganometallic and Organometallic Chemistry. *J. Phys. Chem. A* **2005**, *109*, 11127–11143.

(84) Reiher, M.; Salomon, O.; Hess, B. A. Reparameterization of hybrid functionals based on energy differences of states of different multiplicity. *Theor. Chem. Acc.* **2001**, *107*, 48–55.

(85) Radoń, M. Revisiting the role of exact exchange in the DFT spin state energetics. *Phys. Chem. Chem. Phys.* **2014**, *16*, 14479–14488.

(86) Pinter, B.; Chankisjijev, A.; Geerlings, P.; Harvey, J. N.; Proft, F. D. Conceptual Insights into DFT Spin–State Energetics of Octahedral Transition–Metal Complexes through a Density Difference Analysis. *Chem. Eur. J.* **2018**, *24*, 5281–5292.

(87) Drabik, G.; Radoń, M. Approaching the Complete Basis Set Limit for Spin–State Energetics of Mononuclear First-Row Transition Metal Complexes. *J. Chem. Theory Comput.* **2024**, *20*, 3199–3217.

(88) Peterson, K.; Feller, D.; Dixon, D. Chemical accuracy in ab initio thermochemistry and spectroscopy: current strategies and future challenges. *Theor. Chem. Acc.* **2012**, *131*, 1079.

(89) Weber, R.; Wilson, A. K. Do composite methods achieve their target accuracy? *Computational and Theoretical Chemistry* **2015**, *1072*, 58–62.

(90) Marshall, M. S.; Burns, L. A.; Sherrill, C. D. Basis set convergence of the coupled-cluster correction, δMP2-CCSD(T): Best practices for benchmarking non-covalent interactions and

the attendant revision of the S22, NBC10, HBC6, and HSG databases. *J. Chem. Phys.* **2011**, *135*, 194102.

(91) Gan, Z.; Grant, D. J.; Harrison, R. J.; Dixon, D. A. The lowest energy states of the group-IIIA-group-VA heteronuclear diatomics: BN, BP, AlN, and AlP from full configuration interaction calculations. *J. Chem. Phys.* **2006**, *125*, 124311.

(92) The "aT/D" notation follows ref 87 and the prime symbol denotes the omission of certain function with higher angular momentum, as was detailed above.

(93) Gao, H.; Imamura, S.; Kasagi, A.; Yoshida, E. Distributed Implementation of Full Configuration Interaction for One Trillion Determinants. *J. Chem. Theory Comput.* **2024**, *20*, 1185–1192.

(94) Phung, Q. M.; Nam, H. N.; Saitow, M. Unraveling the Spin-State Energetics of FeN_4 Complexes with Ab Initio Methods. *J. Phys. Chem. A* **2023**, *127*, 7544–7556.

(95) Holmes, A. A.; Umrigar, C. J.; Sharma, S. Excited states using semistochastic heat-bath configuration interaction. *J. Chem. Phys.* **2017**, *147*, 164111.

(96) In order to satisfy the condition $\sigma < u$, we had to adjust in some of these QP2 calculations the parameter `pt2_relative_error`, which expresses the ratio of the allow statistical error to the second-order energy.

(97) Angeli, C.; Cimiraglia, R.; Malrieu, J.-P. *N*-electron valence state perturbation theory: A spinless formulation and an efficient implementation of the strongly contracted and of the partially contracted variants. *J. Chem. Phys.* **2002**, *117*, 9138–9153.

(98) Angeli, C.; Pastore, M.; Cimiraglia, R. New perspectives in multireference perturbation theory: the *n*-electron valence state approach. *Theor. Chem. Acc.* **2007**, *117*, 743–754.

(99) Werner, H.-J. Third-order multireference perturbation theory. The CASPT3 method. *Mol. Phys.* **1996**, *89*, 645–661.

(100) Ghigo, G.; Roos, B.; Malmqvist, P.-Å. A Modified Definition of the Zeroth-Order Hamiltonian in Multiconfigurational Perturbation Theory (CASPT2). *Chem. Phys. Lett.* **2004**, *396*, 142–149.

(101) Neese, F.; Liakos, D.; Ye, S. Correlated wavefunction methods in bioinorganic chemistry. *JBIC J. Biol. Inorg. Chem.* **2011**, *16*, 821–829.

(102) Kepp, K. P. Consistent descriptions of metal–ligand bonds and spin-crossover in inorganic chemistry. *Coord. Chem. Rev.* **2013**, *257*, 196–209.

(103) Urban, M.; Noga, J.; Cole, S. J.; Bartlett, R. J. Towards a full CCSDT model for electron correlation. *J. Chem. Phys.* **1985**, *83*, 4041–4046.

(104) Raghavachari, K.; Trucks, G. W.; Pople, J. A.; Head-Gordon, M. A fifth-order perturbation comparison of electron correlation theories. *Chem. Phys. Lett.* **1989**, *157*, 479 – 483.

(105) Kucharski, S. A.; Bartlett, R. J. Noniterative energy corrections through fifth-order to the coupled cluster singles and doubles method. *J. Chem. Phys.* **1998**, *108*, 5243–5254.

(106) Crawford, T. D.; Stanton, J. F. Investigation of an asymmetric triple-excitation correction for coupled-cluster energies. *Int. J. Quantum Chem.* **1998**, *70*, 601–611.

(107) Noga, J.; Bartlett, R. J. The full CCSDT model for molecular electronic structure. *J. Chem. Phys.* **1987**, *86*, 7041–7050.

(108) Karton, A.; Daon, S.; Martin, J. M. W4-11: A high-confidence benchmark dataset for computational thermochemistry derived from first-principles {W4} data. *Chem. Phys. Lett.* **2011**, *510*, 165–178.

(109) Karton, A. Highly Accurate CCSDT(Q)/CBS Reaction Barrier Heights for a Diverse Set of Transition Structures: Basis Set Convergence and Cost-Effective Approaches for Estimating Post-CCSD(T) Contributions. *J. Phys. Chem. A* **2019**, *123*, 6720–6732.

(110) Řezáč, J.; Šimová, L.; Hobza, P. CCSD[T] Describes Noncovalent Interactions Better than the CCSD(T), CCSD(TQ), and CCSDT Methods. *J. Chem. Theory Comput.* **2013**, *9*, 364–369.

(111) Kállay, M.; Gauss, J. Approximate treatment of higher excitations in coupled-cluster theory. *J. Chem. Phys.* **2005**, *123*, 214105.

(112) Bomble, Y. J.; Stanton, J. F.; Kállay, M.; Gauss, J. Coupled-cluster methods including non-iterative corrections for quadruple excitations. *J. Chem. Phys.* **2005**, *123*, 054101.

(113) Piecuch, P.; Kucharski, S. A.; Kowalski, K. Can ordinary single-reference coupled-cluster methods describe the potential energy curve of N2? The renormalized CCSDT(Q) study. *Chem. Phys. Lett.* **2001**, *344*, 176–184.

(114) Radoń, M.; Drabik, G. Spin States and Other Ligand–Field States of Aqua Complexes Revisited with Multireference Methods Including Solvation Effects. *J. Chem. Theory Comput.* **2018**, *14*, 4010–4027.

(115) Bross, D. H.; Hill, J. G.; Werner, H.-J.; Peterson, K. A. Explicitly correlated composite thermochemistry of transition metal species. *J. Chem. Phys.* **2013**, *139*, 094302.

(116) Vancoillie, S.; Malmqvist, P. Å.; Veryazov, V. Potential Energy Surface of the Chromium Dimer Re-re-revisited with Multiconfigurational Perturbation Theory. *J. Chem. Theory Comput.* **2016**, *12*, 1647–1655.

(117) Li, J.; Yao, Y.; Holmes, A. A.; Otten, M.; Sun, Q.; Sharma, S.; Umrigar, C. J. Accurate many-body electronic structure near the basis set limit: Application to the chromium dimer. *Phys. Rev. Res.* **2020**, *2*, 012015.

(118) Larsson, H. R.; Zhai, H.; Umrigar, C. J.; Chan, G. K.-L. The Chromium Dimer: Closing a Chapter of Quantum Chemistry. *J. Am. Chem. Soc.* **2022**, *144*, 15932–15937.